

PREVALENCE OF TIDAL INTERACTIONS AMONG LOCAL SEYFERT GALAXIES: THE CONTROL EXPERIMENT

YA-WEN TANG

Department of Physics, National Taiwan University, Taiwan and Institute of Astronomy & Astrophysics, Academia Sinica, PO Box 23-141, Taipei 10617, Taiwan

CHENG-YU KUO

Institute of Astronomy & Astrophysics, Academia Sinica, PO Box 23-141, Taipei 10617, Taiwan, and the University of Virginia

JEREMY LIM

Institute of Astronomy & Astrophysics, Academia Sinica, PO Box 23-141, Taipei 10617, Taiwan

AND

PAUL T. P. HO

Institute of Astronomy & Astrophysics, Academia Sinica, PO Box 23-141, Taipei 10617, Taiwan, and the Harvard-Smithsonian Center for Astrophysics

To be submitted to the Astrophysical Journal

ABSTRACT

We test whether there is a relation between the observed tidal interactions and Seyfert activity by imaging in HI twenty inactive galaxies at the same spatial resolution and detection threshold as the Seyfert sample. This control sample of inactive galaxies were closely matched in Hubble type, range in size and inclination, and have roughly comparable galaxy optical luminosity to the Seyfert galaxies. We find that only $\sim 15\%$ of the galaxies in our control sample are disturbed in HI, whereas the remaining $\sim 85\%$ show no disturbances whatsoever in HI. Even at a spatial resolution of ~ 10 kpc, none of the latter galaxies show appreciable HI disturbances reminiscent of tidal features.

In a companion paper (Kuo et al., 2008), we report results from the first systematic imaging survey of Seyfert galaxies in atomic hydrogen (HI) gas. We find that only $\sim 28\%$ of the eighteen Seyfert galaxies in that sample are visibly disturbed in optical starlight. By contrast, $\sim 94\%$ of the same Seyfert galaxies are disturbed spatially and usually also kinematically in HI gas on galactic scales of $\gtrsim 20$ kpc. In at least $\sim 67\%$ and up to perhaps $\sim 94\%$ of cases, the observed disturbances can be traced to tidal interactions with neighboring galaxies detected also in HI. The dramatic contrast between the observed prevalence of HI disturbances in the Seyfert and control samples implicates tidal interactions in initiating events that lead to luminous Seyfert activity in a large fraction of local disk galaxies.

Subject headings: galaxies: active — galaxies: Seyfert — galaxies: interactions — galaxies: structure — galaxies: ISM

1. INTRODUCTION

Active Galactic Nuclei (AGNs) are believed to be manifestations of the vigorous accretion of gas onto a central SuperMassive Black Hole (SMBH). The origin or source of this gas, and how it is brought into the sphere of influence of the SMBH, is one of the longstanding unresolved problems in AGN research (for a recent brief review, see, e.g., Martini, 2004). Only a very small fraction (roughly 1%) of galaxies in the local universe exhibit luminous AGNs, although an appreciable fraction may exhibit non-stellar nuclear activity at some level.

One of the most popular hypothesis for triggering luminous AGNs is gravitational interactions between galaxies. Observational studies of local AGNs have mostly focussed on optically-selected samples of Seyfert galaxies. Seyfert galaxies are preferentially found among early-type spiral galaxies, and exhibit very broad emission lines (from their nuclei) compared with their inactive coun-

terparts. Although most Seyfert galaxies do not appear to be visibly disturbed let alone interacting in optical starlight, some studies report that Seyfert galaxies more frequently possess projected or genuine neighboring galaxies (within a given angular separation) compared with matched samples of inactive galaxies (e.g., Stauffer, 1982; Dahari, 1984; Rafanelli et al., 1995; Dultzin-Hacyan et al., 1999; Koulouridis et al., 2006). This may constitute indirect evidence for more frequent interactions between Seyfert and their neighboring galaxies than their visual appearances would suggest. On the other hand, there also are studies that refute reports of any differences between the frequency of Seyfert and inactive galaxies with projected neighboring galaxies (e.g., MacKenty, 1989; Fuentes-Williams & Stocke, 1988; de Robertis, Yee, & Hayhoe, 1998; Schmitt, 2001).

Studies of nearby galaxies have demonstrated that atomic hydrogen (HI) gas can reveal tidal features not visible in optical starlight (e.g., Yun, Ho, & Lo, 1994). Because the HI disk of normal spiral galaxies usually extends nearly twice as far out as the stellar optical disk, the outer regions of the HI disk is more loosely grav-

Electronic address: ywtang@asiaa.sinica.edu.tw
 Electronic address: ck2v@mail.astro.virginia.edu
 Electronic address: jlim@asiaa.sinica.edu.tw
 Electronic address: pho@asiaa.sinica.edu.tw

itationally bound. The HI disk is therefore more susceptible to external gravitational perturbations than the stellar optical disk, and when perturbed the outskirts also take longer to dynamically relax. This makes HI the most sensitive and enduring tracer known of gravitational interactions between galaxies. To directly address whether Seyfert galaxies are involved in galaxy-galaxy interactions, we have therefore, for the first time, imaged uniformly a relatively large sample of Seyfert galaxies in HI gas. The full results of that study are presented in a companion paper by Kuo et al. (2008). Here, we compare the results of Kuo et al. (2008) with those obtained for a matched sample of inactive galaxies; i.e., a control sample.

To select a control sample, we apply the lessons learnt from optical studies that address whether galaxy-galaxy interactions are responsible for triggering Seyfert activity (see, e.g., discussions in Fuentes-Williams & Stocke, 1988; de Robertis, Yee, & Hayhoe, 1998; Dultzin-Hacyan et al., 1999). A number of the especially earlier studies select as their control sample the closest (in projected separation) inactive galaxies with sizes comparable to the Seyfert galaxy (e.g., Dahari, 1984; MacKenty, 1989; Rafanelli et al., 1995). As pointed by Dultzin-Hacyan et al. (1999), if Seyfert galaxies lie at or close to the center of a local galaxy density enhancement, a control sample selected in this manner may then systematically lie in a region of lower galaxy density. Consistent with this possibility, MacKenty (1989) find that a larger fraction of Seyferts have projected neighboring galaxies than comparably sized inactive galaxies lying in the relatively close vicinity, but not with those selected at random across the sky.

The more recent optical studies select at random inactive galaxies with the same morphological (i.e., Hubble) type and redshift, and sometimes also size and absolute magnitude, as the Seyfert galaxies. This matching is made either on a one-to-one basis (e.g., de Robertis, Hayhoe & Yee, 1998), or over the range of properties observed (e.g., Dultzin-Hacyan et al., 1999). As pointed out by both Fuentes-Williams & Stocke (1988) and Dultzin-Hacyan et al. (1999), matching in absolute magnitudes may systematically bias the control sample to higher luminosities because of the non-negligible contribution from the AGN. An exact match to the absolute magnitude of the Seyfert galaxy minus its AGN contribution is usually not possible as such measurements are not generally available, but is desirable to the degree possible (e.g., as in de Robertis, Yee, & Hayhoe, 1998). By minimizing the differences in galaxy properties between the Seyfert and control samples, it is hoped that a meaningful comparison of their environments will be possible, although this is not obviously the case. Using this method, de Robertis, Yee, & Hayhoe (1998) find no significant excess of projected neighboring galaxies between their Seyfert and control samples, and at best only a marginal difference between their light asymmetries. On the other hand, Dultzin-Hacyan et al. (e.g., 1999) find an excess of Seyfert 2, but not Seyfert 1, with projected neighboring galaxies compared with their control sample, as was later confirmed spectroscopically by Koulouridis et al. (2006).

In our HI imaging study, we select a control sample that is matched on a one-to-one basis in Hubble type,

and which range from lower to approximately the same absolute magnitude as, the sample of active galaxies selected by Kuo et al. (2008). We also matched over the observed range of optical sizes and inclinations. No visual inspection of the control sample was made to see whether they are visibly disturbed, but we are aware that the selection criteria used may select against strongly disturbed galaxies not easily classified in Hubble type. Indeed, using much the same criteria to select their control sample, de Robertis, Hayhoe & Yee (1998) find that a higher proportion of Seyfert galaxies are involved in late-stage mergers than their control sample, although a similar fraction of the control sample displays significant light asymmetries that could be evidence for recent interactions. Note that only a small fraction of the active galaxies studied by Kuo et al. (2008) are visibly disturbed in the optical, but not so strongly that they cannot be classified in Hubble type. Nevertheless, as we shall see, the fraction of optically-disturbed galaxies in the Seyfert sample of Kuo et al. (2008) is higher than that in our control sample. Because our control sample is randomly selected from the field, their environments should be representative (or at least not biased in any peculiar way against those) of inactive galaxies with similar Hubble types, absolute magnitudes, and sizes as the Seyfert sample of Kuo et al. (2008).

In §2 we describe how we selected our control sample of inactive galaxies, and in §3 our HI observations of these galaxies and the data reduction. In §4 we present the results, and in §5 compare these results with those for the Seyfert sample studied by Kuo et al. (2008). In §6, we provide a concise summary of our principle findings and their implications. Unless otherwise specified, we assume throughout a Hubble constant of $H_o = 67 \text{ km s}^{-1} \text{ Mpc}^{-1}$ and $\Omega = 1$ as used by Kuo et al. (2008).

2. SAMPLE SELECTION

As described more fully in Kuo et al. (2008), the parent sample of active galaxies comprise all twenty-seven disk galaxies listed in the Véron-Cetty & Véron (1998), plus another from the Véron-Cetty & Véron (2000), catalog at redshifts of $0.015 \leq z \leq 0.017$ and with absolute B -band magnitudes of $-19 \geq M_B \geq -23$ (for $H_o = 50 \text{ km s}^{-1} \text{ Mpc}^{-1}$, as used in that catalog) in the northern hemisphere ($\delta \geq 0^\circ$). Those galaxies were observed at an angular resolution of $\sim 60''$, which at their distances of 66–75 Mpc corresponds to a spatial resolution of $\sim 20 \text{ kpc}$. The latter is roughly comparable with the optical disk sizes of the active galaxies, and hence the HI observations were tailored towards the detection of structures extended on galactic scales characteristic of tidal features.

Our objective here is to conduct an equivalent HI imaging study of a comparable number of inactive galaxies matched as closely as is reasonably possible to the active galaxy sample. We selected our control sample from the CfA Redshift Survey (Huchra et al., 1983, 1995, see also <http://cfa-www.harvard.edu/~huchra/zcat/>) according to the following criteria.

1. Redshift: to reduce the required observing time (which amounted to an integration time of 2 hrs and an observing time of ~ 2.5 hrs per object in our

active galaxy sample), we selected inactive galaxies at half the redshift range of our active galaxy sample; i.e., at $0.0075 \leq z \leq 0.0085$ (distance of 33.4–37.8 Mpc). A total of 166 galaxies in the CfA redshift catalog met this criterion.

Individual samples selected in optical studies are located over a much broader range of redshifts, making one-to-one (or overall) matching in redshift (range) important for avoiding difficulties when looking for an excess of projected neighboring galaxies between two samples. Here, our objective is to search for large-scale HI disturbances in our target galaxies, and determine whether these disturbances are produced by tidal interactions with neighboring galaxies. In such a case, matching in redshift is not necessary so long as we observe both samples at the same spatial resolution and detection threshold (see §3), and provided there is no significant Cosmological evolution between the two redshifts. Of course, to look for interacting neighboring galaxies (but not necessarily to detect tidal features in the target galaxies), in both samples the field of view has to be sufficiently large to encompass any such galaxies.

2. Optical morphology and luminosity: from the parent sample of 166 inactive galaxies, we matched on a one-to-one basis the Hubble type and optical *B*-band luminosity of each active galaxy to one or more inactive galaxies. Both the optical morphology and luminosity were taken from Leda, now renamed the Hyperleda database (<http://leda.univ-lyon1.fr>; Paturel et al., 2003). The morphology is matched to an accuracy of one Hubble subtype (e.g., for an Sa active galaxy, we matched to S0a-Sab inactive galaxies) given the inherent fuzziness in morphological classifications. Because the absolute magnitudes of the active galaxies include a poorly determined contribution from their bright nuclei, we allowed the match in absolute magnitude to be up to one magnitude larger (i.e., optical *B*-band luminosity up to a factor of 2.5 lower) than that of the corresponding active galaxy.
3. Optical size and inclination: based once again on the Hyperleda database, we also loosely matched in optical size by restricting the galaxy diameters to the range $\sim 0.8\text{--}4.3$ (with the majority in the range $\sim 1.5\text{--}2.5$) as measured at the 25 mag arcsec⁻² isophotal level in the *B*-band. This range in angular diameters is roughly comparable with the corresponding range in physical diameters of the active galaxy sample. Because none of the active galaxies are close to face on (i.e., inclinations close to 0°), we also restricted the inclinations of the inactive galaxies to angles $\geq 26^\circ$ with respect to the plane of the sky.
4. Radio continuum: to avoid the effect in our dynamic range of our maps, we discarded those galaxies that lie near bright radio continuum sources detected in the NRAS VLA Sky Survey (NVSS; Condon et al. 1998) which would appear in the field of view of our HI observations. Here, we set a flux

density cut at 21 cm of 1000 mJy. The detected flux densities of both sample and its companions are in the order of 100 mJy. This cut will not cause any bias when comparing results of the seyfert and control sample.

In this way, we selected twenty-seven inactive galaxies that are closely matched in Hubble type and to the degree possible absolute magnitude, as well as range in size and inclination, to the sample of twenty-eight active galaxies in Kuo et al. (2008). The basic properties of this matched control sample are listed in Table 1. Note that some of the values originally obtained from the Leda database have since been updated in the Hyperleda database; we list the latest, and presumably most reliable, values from the Hyperleda database. Our selection is entirely blind to the HI content of these galaxies.

In Figure 1, we plot the number distribution in morphological types, absolute magnitudes, optical sizes, and inclinations of both the active galaxy sample in Kuo et al. (2008) and our control sample. The number distribution in morphological types (top panel) shows no marked differences between the two samples within a precision of a Hubble subtype; a Kolmogorov-Smirnov (K-S) test applied to the two samples gives a K-S statistic $D = 0.18$ (converging to 0 for identical distributions) and probability $\text{Pr} = 0.74$ (1 for identical distributions). As intended, the absolute magnitudes (second panel from top) of the control sample are skewed towards larger values (i.e., lower luminosities) than the active sample. The distribution in optical sizes also is skewed towards somewhat smaller dimensions for the control sample, but the majority in both samples span the same range. The control sample has more moderately inclined ($30^\circ\text{--}45^\circ$) than high inclined ($75^\circ\text{--}90^\circ$) galaxies compared to the active sample, but once again the majority in both samples span the same range. The relatively small differences seen between the distribution of physical properties between the active and control samples should not have a significant effect on the detectability of HI tidal features in the two samples; as shown by Kuo et al. (2008), the vast majority of the active galaxies, and nearly all those classified as Seyferts, exhibit HI disturbances usually in the form of tidal features irrespective of their Hubble type, absolute magnitude, optical size, or inclination within the selected range.

3. OBSERVATIONS AND DATA REDUCTION

We observed the control sample with the Very Large Array (VLA) of the National Radio Astronomical Observatory (NRAO). Like the active galaxy sample studied by Kuo et al. (2008), we used the most compact configuration of the VLA (the D-array). NGC 5375 had previously been adequately (for the purpose of this experiment) observed in this configuration on 1996 August 15, and so we simply retrieved the data for this galaxy from the VLA archive. The remaining galaxies were observed on 2003 February 19, 21, and 24, apart from NGC 5355 which was observed on 2004 July 14. Other relevant details of the observations, including the flux, secondary (for amplitude and phase calibration), and bandpass calibrators used for each target object, are summarized in Table 2.

The correlator was configured in the same manner described in Kuo et al. (2008), recording signals in orthogo-

nal circular polarizations in sixty-four channels spanning a bandwidth of 6.25 MHz. The corresponding channel separation in velocity is $\sim 21.2 \text{ km s}^{-1}$ (the actual velocity resolution is $\sim 25.2 \text{ km s}^{-1}$), and altogether span a velocity range of $\sim 1350 \text{ km s}^{-1}$. For the assumed Cosmology, this velocity range corresponds to a redshift interval of $\Delta z \approx 0.0045$ (distance range of $\sim 20 \text{ Mpc}$), compared with the redshift interval of $\Delta z \approx 0.001$ for the control sample. The central channel is set to the systemic heliocentric velocity of the HI line if previously measured (usually with a single-dish telescope), or if not then at its reported optical redshift.

At 21 cm, the primary beam of the VLA is $\sim 32'$ at full-width half-maximum, corresponding to a diameter of $\sim 330 \text{ kpc}$ at the distance of our control sample. Our field of view for the control sample is, of course, only half the linear diameter of our field of view for the active galaxy sample, which is located at twice the distance. As described in Kuo et al. (2008), the projected separation between the Seyfert and their interacting neighboring galaxies is mostly (for $\sim 85\%$ of the sample) $\lesssim 100 \text{ kpc}$. Our field of view is therefore sufficiently large to encompass most of the interacting neighboring galaxies detected around the Seyfert galaxies studied by Kuo et al. (2008) even if the latter was placed at the distance of our control sample.

We targeted the same detection threshold at the same spatial resolution as Kuo et al. (2008) for their active galaxy sample. Because the control sample is a factor of two closer in distance, their HI intensity is a factor of 4 higher for the same gas mass. Everything else being equal, this would require a factor of 16 shorter integration time for our control sample, a considerable saving given that the integration time for each active galaxy in Kuo et al. (2008) was $\sim 2 \text{ hrs}$. In practise, to achieve the same spatial resolution of $\sim 20 \text{ kpc}$ (i.e., angular resolution of $\sim 120''$) as in the active galaxy sample (which was imaged at an angular resolution of $\sim 60''$), we had to discard baselines that were more than one-third the length of the longest baselines in the active galaxy sample (i.e., using baseline up to only $1.5 \text{ k}\lambda$). Because there are more shorter than longer baselines, the actual integration time per object in our control sample was therefore $\sim 12 \text{ mins}$ (still a considerable saving in time over 2 hrs) and the observing time per object $\sim 20 \text{ mins}$ (compared with $\sim 2.5 \text{ hrs}$ for the active galaxy sample). In this way, we achieved a rms flux density of $\sim 1.8 \text{ mJy beam}^{-1}$ in one channel, corresponding to a 5σ detection threshold in HI gas column density of $\sim 3 \times 10^{19} \text{ cm}^{-2}$ per synthesized beam of diameter $\sim 120''$ (20 kpc) in a given channel with a velocity width $\sim 25.2 \text{ km s}^{-1}$. This is the same detection threshold as reached by Kuo et al. (2008) in their active galaxy sample.

Like Kuo et al. (2008), we performed all the data reduction in the standard manner using the NRAO AIPS package. Unlike for the active galaxy sample, we found no radio frequency interference (RFI) in the data for our control sample, presumably because their redshifted HI lines lie closer to the protected band at 21 cm. Following bandpass calibration, as well as time-dependent amplitude and phase calibration, we subtracted the continuum emission from the visibility data by interpolating between line-free channels (determined through trial and error) on either side of the HI line. For NGC 4256, where

there is a relatively strong continuum source in the field, we first subtracted the continuum emission of that source in the visibility plane. Finally, we made maps of each channel, and corrected for the primary beam response of the antennas. We also combined the channel maps (before primary beam correction) to make maps in total intensity (zeroth moment) and intensity-weighted mean velocity (first moment), where we tried several different combinations of spectral smoothing and minimum signal cutoff level in each channel so as to suppress the noise and bring out faint diffuse features.

4. RESULTS

We detected twenty-one of the twenty-seven galaxies in our control sample. Two of the six galaxies not detected, NGC 4128 and NGC 4543, have (to the best of our knowledge) not previously been observed in HI. The reported upper limits in the integrated HI intensities for NGC 4578 (Huchtmeier et al. 1998) and NGC 5326 (Theureau et al. 1998) are below that attained in our observations. NGC 3468 has a reported integrated HI intensity of $1.40 \text{ Jy km s}^{-1}$ (with no reported uncertainty) in Huchtmeier (1989), and should therefore have been detected in our observation. On checking the original source of the detection in Giovanelli & Haynes (1981), we found that the actual galaxy detected was UGC 3468 and not NGC 3468 as reported in Huchtmeier (1989). NGC 5355 has a reported integrated HI intensity of $14.6 \pm 1.8 \text{ Jy km s}^{-1}$ in Huchtmeier (1989), and should therefore have been detected in our observation. On checking the original source of the detection, Richter and Huchtmeier (1991) mentioned that the $8/8$ beam of the Effelsburg telescope used for this observation would include also NGC 5353 and NGC 5354. We note that this beam also includes NGC 5350, which is one of the galaxies in our control sample. We detected NGC 5350 at a much higher integrated HI intensity than that reported by Richter and Huchtmeier (1991) for NGC 5355, suggesting that the actual HI detection was of NGC 5350.

The twenty-one galaxies that we detected in HI comprise our ensemble control sample from which we draw statistical results. For comparison, there are twenty-three active galaxies in the ensemble sample of Kuo et al. (2008), of which eighteen are classified as Seyfert galaxies. The HI maps of the ensemble control sample are shown in Figures 2–25, and their HI properties summarized in Table 3. We have overlaid each integrated HI intensity (zeroth moment) map on an optical (either the red or blue filters) image from the 2nd Digitized Sky Survey (DSS2). This database provides a relatively uniform set of optical images to search for any disturbances in optical starlight.

We also detected in HI a number of galaxies in the same field of view as our target galaxies. Those galaxies lying within the primary beam (i.e., within a radius of $\sim 15/8$ about phase center) are listed in Table 4, and are referred to by their names from optical catalogs. We also list their optical redshifts where available, as well as their corrected apparent B -band magnitudes and Hubble types as listed in the Hyperleda database. The measured HI properties of these neighboring galaxies are summarized in Table 5. Apart from neighboring galaxies detected in HI, we also searched the Hyperleda database in a radius of $\sim 15'$ about each galaxy in our control sample

to obtain a measure of the richness of their fields. We emphasize that this is by no means an exhaustive search.

4.1. Individual Galaxies

We present here the results for each galaxy, highlighting features of most relevance to this work. As in Kuo et al. (2008), we separate the individual galaxies in our ensemble control sample into the following three groups.

1. Those that clearly show HI tidal features tracing interactions with neighboring galaxies. These features are in the form of tidal bridges that connect the two interacting galaxies, or an extension from one or both galaxies in the direction of the other (i.e., an incomplete tidal bridge). In addition, features in the form of tidal tails comprising a protrusion or curved extension from one galaxy on the side away from the other interacting galaxy may be seen. Only one of the twenty-one galaxies in our ensemble control sample of inactive galaxies fall into this group. By comparison, thirteen of the twenty-three galaxies in the ensemble sample of active galaxies, including twelve of the eighteen classified as Seyferts, fall into this group.
2. Those that clearly show both spatial and kinematic disturbances in HI, but which cannot be directly linked to interactions with neighboring galaxies if any. These disturbances are in general less prominent than the tidal features observed in the first group. Only two of the twenty-one galaxies in our ensemble control sample of inactive galaxies fall into this group. Four of the twenty-three galaxies in the ensemble sample of active galaxies, including three of the eighteen classified as Seyferts, fall into this group.
3. Those that show marginal or no detectable HI disturbances. Eighteen of the twenty-one galaxies in our ensemble control sample of inactive galaxies fall into this group. Only one exhibits weak HI disturbances; the remaining seventeen exhibit no discernible HI disturbances. By comparison, only six of the twenty-three galaxies in the ensemble sample of active galaxies, including only three (two of which exhibit weak HI disturbances) of the eighteen classified as Seyferts, fall into this group.

Because the vast majority of the galaxies in our control sample exhibit no detectable HI disturbances at an angular resolution of $\sim 120''$ (~ 20 kpc), for these undisturbed galaxies we show only HI maps at the full angular resolution attained in our observations of $\sim 60''$ (~ 10 kpc). The maps at $\sim 120''$ angular resolution contain no extra information. For the disturbed galaxies, moment maps are shown at angular resolutions of both $\sim 120''$ and $\sim 60''$ for the reader to compare, and HI channel maps at an angular resolution of $\sim 120''$ only. The HI channel maps of the undisturbed galaxies are available in the electronic version of this paper (Figs. 28–44). (For astroph readers, the channel maps are available at the link <http://www.astro.virginia.edu/~ck2v/maps>) At an angular resolution of $\sim 60''$, the corresponding 5σ detection threshold in HI gas column density is $\sim 7 \times 10^{19} \text{ cm}^{-2}$

per synthesized beam in a given channel with a velocity width $\sim 25.2 \text{ km s}^{-1}$, which is higher than the Seyfert sample. Because the Seyfert sample is twice further away from us comparing with the control sample, the detection limit in terms of the HI mass of the control sample ($\sim 6 \times 10^7 M_\odot$) is lower than of the seyfert sample ($\sim 7 \times 10^8 M_\odot$).

4.1.1. Group I: HI tidal features tracing interactions with neighboring galaxies

At a spatial resolution of ~ 20 kpc only one of our ensemble sample of inactive galaxies exhibit tentative HI disturbances, which only in the map at a spatial resolution of 10 kpc can be clearly seen to trace to tidal interactions with neighboring galaxies. Nevertheless, we generously place this sole example of its kind in Group 1. When categorizing the ensemble sample of active galaxies in Kuo et al. (2008), we took a more conservative approach.

NGC 2543

NGC 2543 is a barred Sb galaxy (all Hubble types from the Hyperleda database, just as for the active galaxies in our companion paper). It appears somewhat asymmetric in the optical, although not obviously disturbed. A relatively dim galaxy at a comparable optical redshift, PGC 80408, lies $\sim 3.4'$ (~ 36 kpc) south of NGC 2543.

Our HI image at a spatial resolution of ~ 20 kpc (Fig. 2) reveals that NGC 2543 shares a common envelope with PGC 80408. An examination of the channel maps at this spatial resolution (Fig. 3) reveals tentative evidence for a tidal bridge (which, if real, is at best marginally spatially resolved) connecting the two galaxies. Our HI image at a spatial resolution of ~ 10 kpc (also shown in Fig. 2), and also the channel maps at this angular resolution (also Fig. 3), clearly reveals that the connection between the two galaxies is indeed a tidal bridge. In addition, the HI disk of NGC 2543 is clearly disturbed on its southwestern side, which on this side extends much further than on the north-eastern side and curls in a direction towards its interacting neighbour PGC 80408.

4.1.2. Group II: HI disturbances likely produced by interactions

Two of the galaxies in our ensemble control sample exhibit spatial and kinematic disturbances in HI, but unlike the situation in Group I the observed perturbations cannot be immediately linked to interactions with neighboring galaxies.

NGC 2551

NGC 2551 is a Sa galaxy. A dimmer galaxy at a comparable optical redshift, UGC 4390, lies $\sim 14.4'$ (~ 146 kpc) to the north-east of NGC 2551. Neither galaxies appear to be visibly disturbed in the optical.

We detected both NGC 2551 and UGC 4390 in HI, as well as the relatively faint galaxy PGC 2755603, which has no previously reported optical redshift (Figs. 4 and 5). At a spatial resolution of ~ 20 kpc (Fig. 5), the HI disk of NGC 2551 appears to be disturbed, with this disturbance especially prominent in the first moment

map (kinematics). The observed disturbance in the HI disk is even more prominent at an angular resolution of ~ 10 kpc (Fig. 4), but not easily apparent in the channel maps (Fig. 6). By comparison, UGC 4390 does not appear to be disturbed in HI at either spatial resolutions, although it is possible that the HI kinematic axis is not aligned with the optical major axis (the optical major axis is poorly defined in the outer regions of this galaxy). PGC 2755603 was not spatially resolved in HI. It is not clear whether the observed disturbance in NGC 2551 was caused by tidal interactions with (one of) these or other galaxies.

NGC 3094

NGC 3094 is a barred Sa galaxy that does not appear to be obviously disturbed in the optical. In HI (Fig. 7), we detected NGC 3094 and also PGC 2806972, a relatively faint galaxy that lies ~ 7.5 (~ 78 kpc) to the east of NGC 3094. PGC 2806972 has no previously reported optical redshift.

NGC 3094 exhibits a HI protrusion on the south-eastern side that is kinematically discontinuous from its HI disk. A close examination of the channel maps (Fig. 8) reveals that this protrusion is physically linked to NGC 3904. These channel maps also reveal prominent north-south extensions over a narrow velocity range not seen in the moment maps; these extensions are orthogonal to the HI kinematic axis of the galaxy. There are no cataloged galaxies at the location of this protrusion, nor any optical counterpart visible in the DSS2 image. It is possible that this protrusion is an incomplete tidal bridge caused by interactions with PGC 2806972.

4.1.3. Group III: Weak or no HI disturbances

Eighteen of the twenty-one galaxies fall into this group, accounting for the vast majority of the galaxies in our ensemble control sample. Of these eighteen, seventeen do not show any evidence whatsoever for disturbances in HI. Only NGC 3976, which as we explain below has recently been classified as an active galaxy, shows evidence for weak disturbances.

NGC 3976

NGC 3976 is a barred Sb galaxy. It is clearly disturbed in the optical (Fig. 9), exhibiting asymmetric extensions on the north-eastern and south-western sides of the disk. Although NGC 3976 is not classified as an active galaxy by Véron-Cetty & Véron (1998), the source used to select the active galaxy sample, it is classified as a Seyfert 2 with $M_B = -21.1$ in the latest version of this catalog (Veron-Cetty & Veron, 2006). Thus, if NGC 3976 was placed at the same range of redshifts as the active galaxy sample, it would have been selected as part of that sample. For internal consistency, however, we retain NGC 3976 in our control sample. If included in the active galaxy sample, this would make the conclusions reached in our study only stronger. A relatively faint galaxy at a comparable optical redshift, PGC 37490, lies ~ 4.5 to the south of NGC 3976.

We detected NGC 3976, but not PGC 37490. At a spatial resolution of ~ 20 kpc, the HI disk of NGC 3976 appears to be asymmetric (Fig. 9). The HI gas extends

further out on the north-eastern side compared to the south-western side, giving the disk a lopsided appearance in HI. In addition, the HI kinematic axis appears to lie at a different position angle compared with the major axis of the optical disk. At a spatial resolution of ~ 10 kpc (also shown in Fig. 9), this asymmetric appearance appears to be caused in part (but perhaps not wholly) by the larger HI extension of the north-eastern compared with the south-western spiral arm.

IC 2461

IC 2461 is an edge-on Sb galaxy that does not appear to be visibly disturbed in the optical. There are no cataloged galaxies at a comparable optical redshift within $15'$ of the galaxy.

At a spatial resolution of ~ 20 kpc, the HI disk of IC 2461 appears to be symmetric both spatially and kinematically with no evidence for perturbations. At a spatial resolution of ~ 10 kpc (Fig. 10), the HI major and kinematic axes appears to exhibit an anticlockwise twist on the north-western side of the disk, perhaps indicative of a warp.

NGC 3835

NGC 3835 is a Sab galaxy that is not visibly disturbed in the optical. There are no cataloged galaxies at a comparable optical redshift within $15'$ of the galaxy.

At a spatial resolution of ~ 20 kpc, the HI disk of NGC 3835 appears to be symmetric both spatially and kinematically with no evidence for perturbations. The same also is true at a spatial resolution of ~ 10 kpc (Fig. 11), where the central inward contraction of the intensity contours in the zeroth moment maps is probably caused by a depression in HI intensity at the center of the galaxy (as is often observed in nearly disk galaxies).

NGC 4067

NGC 4067 is a Sb galaxy that is not visibly disturbed in the optical. There are no cataloged galaxies at a comparable optical redshift within $15'$ of the galaxy.

At a spatial resolution of ~ 20 kpc, the HI disk of NGC 4067 appears to be symmetric both spatially and kinematically with no evidence for perturbations. At a spatial resolution of ~ 10 kpc (Fig. 12), the HI disk appears to be more prominent or extended on the south-western side compared with the north-eastern side. Other than this small asymmetry, the HI disk does not exhibit any spatial nor kinematic disturbances. Once again, the central inward contraction of the intensity contours in the zeroth moment maps is probably caused by a depression in HI intensity at the center of the galaxy.

NGC 4256

NGC 4256 is an edge-on Sb galaxy that is not visibly disturbed in the optical. There are five relatively faint cataloged galaxies at a comparable optical redshift within $15'$ of NGC 4256. Their separations range from 0.4 (~ 4 kpc) to $14'$ (~ 153 kpc) from NGC 4256. None of these neighboring galaxies were detected in HI.

The HI gas mass of NGC 4256 is the lowest among all of the galaxies in our ensemble control sample, and hence the corresponding signal-to-noise ratio of the HI map for this galaxy poorest. At a spatial resolution of ~ 20 kpc, the HI disk of NGC 4256 appears to be symmetric both spatially and kinematically with no evidence for perturbations. The same also is true at a spatial resolution of ~ 10 kpc (Fig. 13).

NGC 4275

NGC 4275 is a Sb galaxy that has the smallest inclination among all of the galaxies in our ensemble control sample. There are no cataloged galaxies at a comparable optical redshift within $15'$ of the galaxy.

At a spatial resolution of ~ 20 kpc, the HI disk of NGC 4275 appears to be symmetric both spatially and kinematically with no evidence for perturbations. The same also is true at a spatial resolution of ~ 10 kpc (Fig. 14).

NGC 4351

NGC 4351 is a barred Sab type galaxy that appears to be disturbed in the sense that it is lopsided in the optical, being more extended on the western than eastern side of the galaxy. There are no cataloged galaxies at a comparable optical redshift within $15'$ of the galaxy.

At a spatial resolution of ~ 20 kpc, the HI disk of NGC 4351 appears to be symmetric both spatially and kinematically with no evidence for perturbations. At a spatial resolution of ~ 10 kpc (Fig. 15), the HI disk is asymmetric in that it is more prominent or extended on the western side, just like in the optical.

NGC 4384

NGC 4384 is a Sa galaxy that is not visibly disturbed in the optical. There is a relatively faint galaxy, PGC 2478952, with a comparable optical redshift at $\sim 14'.9$ (~ 162 kpc) from NGC 4384. That galaxy was not detected in HI.

At a spatial resolution of ~ 20 kpc, the HI disk of NGC 4384 appears to be symmetric both spatially and kinematically with no evidence for perturbations. At a spatial resolution of ~ 10 kpc (Fig. 16), the HI disk may be somewhat asymmetric in that the eastern side appears to be more prominent or extended.

NGC 4470

NGC 4470 is a Sa type galaxy that is not visibly disturbed in the optical. The galaxy that is closest in optical redshift and which lies within $15'$ of NGC 4470 differs in systemic velocity by ~ 900 km s $^{-1}$, and lies outside the velocity coverage of our HI observation.

At a spatial resolution of ~ 20 kpc, the HI disk of NGC 4470 appears to be symmetric both spatially and kinematically with no evidence for perturbations. At a spatial resolution of ~ 10 kpc, the HI disk may show weak asymmetries (Fig. 17).

NGC 4513

NGC 4513 is a S0 galaxy that is not visibly disturbed in the optical. There are no cataloged galaxies at a comparable optical redshift within $15'$ of the galaxy.

At a spatial resolution of ~ 20 kpc, the HI disk of NGC 4513 appears to be symmetric both spatially and kinematically with no evidence for perturbations. The same also is true at a spatial resolution of ~ 10 kpc (Fig. 18). This galaxy has the second lowest HI gas mass among our ensemble control sample, with the resulting low signal-to-noise ratio making the presumed central depression in HI gas particularly prominent.

NGC 4567 and NGC 4568

Both NGC 4567 and NGC 4568 are Sbc galaxies that form an optically-overlapping pair with comparable optical redshifts. In this way, NGC 4567/NGC 4568 resemble UGC 3995/UGC 3995A in the active galaxy sample. Both NGC 4567 and NGC 4568 are included in our control sample. There are no other cataloged galaxies at a comparable optical redshift within $15'$ of the galaxy.

Despite their apparent proximity and similar redshifts, as in the case of UGC 3995/UGC 3995A we detect no HI disturbances at a spatial resolution of ~ 20 kpc, nor at a spatial resolution of ~ 10 kpc (Fig. 19), in either NGC 4567 or NGC 4568. Indeed, in a much deeper HI observation at an angular resolution of $\sim 20''$, Iono et al. (2005) detected no extended tidal features in this pair of galaxies.

NGC 4591

NGC 4591 is a Sb galaxy that is not visibly disturbed in the optical. There are no cataloged galaxies at a comparable optical redshift within $15'$ of the galaxy.

At a spatial resolution of ~ 20 kpc, the HI disk of NGC 4591 appears to be symmetric both spatially and kinematically with no evidence for perturbations. The same also is true at a spatial resolution of ~ 10 kpc (Fig. 20).

NGC 4814

NGC 4814 is a Sb galaxy that is not visibly disturbed in the optical. There is a relatively faint galaxy, SDSSJ 125426.85+582348.9, with a comparable optical redshift at $\sim 7'.9$ (~ 86 kpc) from NGC 4384. That galaxy was not detected in HI.

At a spatial resolution of ~ 20 kpc, the HI disk of NGC 4814 appears to be symmetric both spatially and kinematically with no evidence for perturbations. The same also is true at a spatial resolution of ~ 10 kpc (Fig. 21).

NGC 4964

NGC 4964 is a S0-a galaxy that is not visibly disturbed in the optical. There are no cataloged galaxies at a comparable optical redshift within $15'$ of the galaxy.

At a spatial resolution of ~ 20 kpc, the HI disk of NGC 4964 appears to be symmetric both spatially and kinematically with no evidence for perturbations. The same also is true at a spatial resolution of ~ 10 kpc (Fig. 22).

NGC 5289

NGC 5289 is a nearly edge-on barred Sa galaxy that is not visibly disturbed in the optical. There are six mostly relatively faint cataloged galaxies at a comparable optical redshift within $15'$ of NGC 5289. Their separations range from $5.3'$ (~ 58 kpc) to $12.7'$ (~ 138 kpc) from NGC 5289. Only of these neighboring galaxies, NGC 5290, lying furthest away from and brighter in the optical than NGC 5289, was detected in HI.

At a spatial resolution of ~ 20 kpc, the HI disk of NGC 5289 appears to be symmetric both spatially and kinematically with no evidence for perturbations. The same also is true at a spatial resolution of ~ 10 kpc (Fig. 23).

NGC 5350

NGC 5350 is a barred Sbc galaxy that appears to be somewhat asymmetric although not obviously disturbed in the optical. There are seven cataloged galaxies at a comparable optical redshift within $15'$ of NGC 5350, two of which are comparably bright and the remainder relatively faint. None of these neighboring galaxies were detected in HI.

At a spatial resolution of ~ 20 kpc, the HI disk of NGC 5350 appears to be symmetric both spatially and kinematically with no evidence for perturbations. The same also is true at a spatial resolution of ~ 10 kpc (Fig. 24).

NGC 5375

NGC 5375 is a barred Sab galaxy that is not visibly disturbed in the optical. There is a relatively faint galaxy, PGC 49623, with a comparable optical redshift at $\sim 4.6'$ (~ 47 kpc) from NGC 5375. That galaxy was not detected in HI. Instead, we detected the galaxy MAPS-NGP O-325-1536477 (as cataloged in the NASA Extragalactic Database), which has no previously reported optical redshift, which is $9.4'$ (~ 131 kpc) to the south-east of NGC 5375.

At a spatial resolution of ~ 20 kpc, the HI disk of NGC 5375 appears to be symmetric both spatially and kinematically with no evidence for perturbations. The same also is true at a spatial resolution of ~ 10 kpc (Fig. 25).

4.2. Other Galaxies in Target Fields

Apart from the optically-overlapping pair NGC 4567/NGC 4568, we detected only six other galaxies in HI within the primary beam of our target fields. None of these galaxies exhibit HI disturbances at either 20 kpc or 10 kpc spatial resolution. The HI maps of these galaxies are shown together with the maps for the control sample galaxies.

4.3. Ensemble Statistics

We now make statistical inferences from the results based on our ensemble control sample of twenty-one galaxies that we mapped in HI. Only four of the twenty-one ($\sim 19\%$) galaxies in the control sample exhibit detectable disturbances at a spatial resolution of ~ 20 kpc.

By contrast, seventeen of the twenty-one ($\sim 81\%$) galaxies exhibit no HI disturbances whatsoever at this spatial resolution. One of these disturbed galaxies (NGC 3976) has since been found to be a Seyfert 2 galaxy, and so only three of the twenty (15%) inactive galaxies are actually disturbed in HI, whereas seventeen of twenty ($\sim 85\%$) show no HI disturbances. The HI disturbances be directly traced to tidal interactions with neighboring galaxies in only one case. In the remaining two cases with HI disturbances, the observed disturbances are likely to be produced by tidal interactions with neighboring galaxies also detected in HI. By comparison, seventeen of the eighteen ($\sim 94\%$) Seyfert galaxies in the ensemble sample of Kuo et al. (2008) exhibit HI disturbances, twelve ($\sim 67\%$) of which are interacting with neighboring galaxies (Group I), another three ($\sim 17\%$) probably interacting with neighboring galaxies (Group II), and the remaining two ($\sim 12\%$) weakly disturbed (Group III).

Only two of the twenty-one ($\sim 10\%$) galaxies in the control sample are visibly disturbed in optical DSS2 images. Leaving aside NGC 3976 since found to be a Seyfert 2 galaxy, only one of twenty ($\sim 5\%$) inactive galaxies are optically disturbed. By comparison, six of the twenty-three ($\sim 26\%$) galaxies in the ensemble sample of active galaxies studied by Kuo et al. (2008) are visibly disturbed in optical DSS2 images, including five of the eighteen galaxies ($\sim 28\%$) classified as Seyferts. As pointed out in § 1, the selection criteria used may select against (strongly) optically disturbed galaxies in the control sample. Nonetheless, the relatively small difference in the frequency of optical disturbances between the Seyfert and control samples ($\sim 28\%$ vs $\sim 5\%$) pales besides the dramatic difference in the frequency of HI disturbances between these two samples ($\sim 94\%$ vs $\sim 15\%$).

In case of any severe selection bias against optically-disturbed galaxies in our control sample, here we compile statistics for just the optically-undisturbed galaxies in both the Seyfert and control sample. Of the thirteen such Seyfert galaxies, twelve ($\sim 92\%$) exhibit HI disturbances, nine ($\sim 69\%$) of which are interacting with neighboring galaxies (Group I), one ($\sim 7\%$) possibly interacting with a neighboring galaxy (Group II), and two ($\sim 15\%$) weakly disturbed (Group III). By comparison, only three of the twenty ($\sim 15\%$) optically-undisturbed inactive galaxies are disturbed in HI.

5. INTERPRETATION AND DISCUSSION

5.1. Relative HI Gas Masses

We first examine whether the dramatic difference in HI disturbances between the active and control samples might be caused by differences in their HI gas masses. This could happen if, for example, the same fractional HI gas mass is displaced into tidal features of equal spatial dimensions in a given interaction. In such a case, interacting galaxies with lower HI gas masses will exhibit dimmer tidal features, which may fall below the detection threshold in a given observation.

In Figure 26, we plot the HI gas masses of the active and control samples. As can be seen, the active sample is distributed towards somewhat higher HI gas masses than the control sample. A K-S test gives a statistic $D = 0.30$ (converging to 0 for identical distributions) and probability $\text{Pr} = 0.23$ (1 for identical distributions). More importantly, most of the galaxies in our control sample

span the same range of HI gas masses as the active sample for which we detect HI disturbances. We therefore believe that the dramatic difference in HI disturbances between the two samples cannot be caused by the relatively small difference in their overall distributions of HI gas masses. The possibility that tidal features in our control sample somehow conspire to be less spatially extended than those in the active sample is ruled out by our HI images of the control sample at a spatial resolution of ~ 10 kpc.

5.2. Incidence of Neighboring Galaxies

In Figure 27, we show the cumulative fraction of Seyfert galaxies (solid line) studied by Kuo et al. (2008) with (candidate) interacting neighboring galaxies (i.e., in Groups I, II, or III), plotted as a function of their projected separations (for the few with multiple interacting neighboring galaxies, their nearest such neighbor). As explained in Kuo et al. (2008), over the range of projected separations plotted (up to 90 kpc), there are only two neighboring galaxies not identified to be (possibly) interacting with their respective (the same) Seyfert galaxy, the third of which is identified as the interacting neighbor. Thus, including all possible neighboring galaxies around Seyfert galaxies do not change this figure, at least within the range of projected separations plotted. In the same figure, we also plot the cumulative fraction of galaxies in our control sample (dashed line) with neighboring galaxies within the same range of projected separations. (Keep in mind that our observations span the same velocity interval for both samples.) Our detection threshold is relatively uniform (within $\sim 20\%$) and essentially the same for both the Seyfert and control samples at projected separations up to ~ 90 kpc. As can be seen, the frequency of Seyfert with neighboring galaxies is clearly much higher than that of the control sample over the range of projected separations plotted. This difference simply reflects the prevalence of tidal interactions in the Seyfert but not control sample.

As mentioned in §1, some optical studies find an excess of Seyfert with (projected) neighboring galaxies compared with inactive galaxies, whereas others do not. A discussion of the different methodologies used in different studies, as well as reasons for their conflicting results, is beyond the scope of this paper. Any comparison made between previous optical and our HI studies should keep in mind that our HI imaging study is not designed to address differences between the fraction of Seyfert and inactive galaxies with neighboring galaxies. (Rather than looking for any such difference, we directly determine what fraction of Seyfert and inactive galaxies show HI disturbances, and where possible determine whether these disturbances are caused by tidal interactions with neighboring galaxies.) Both the study of Kuo et al. (2008) and that reported here can only detect relatively gas-rich galaxies, and so a HI census of neighboring galaxies is likely to be less complete than an optical census.

Nevertheless, to see what can be learnt, we compare the results of our HI studies with the optical studies of Dultzin-Hacyan et al. (1999) and Koulouridis et al. (2006), who measured the fraction of galaxies in both their Seyfert and control samples with (projected) neighboring galaxies as a function of their projected separa-

tions. Both these studies employed the same Seyfert and control samples; the Seyfert sample was taken from the catalog of Lipovetsky et al. (1988), which contained most if not all of the then known Seyfert galaxies, and the matched control sample from the CfA survey (Huchra et al., 1983).

Dultzin-Hacyan et al. (1999) searched for projected neighboring galaxies within a radius of ~ 140 kpc using the (first) Digitized Sky Survey (DSS). They found that in both their Seyfert and control samples, the fraction having projected neighboring galaxies with diameters 4–10 kpc increases as the search radius widens, reaching between 80%–100% within a search radius of ~ 100 kpc (see Fig. 1 of Dultzin-Hacyan et al., 1999). At any given search radius, the fraction of Seyfert 1 and inactive galaxies possessing projected neighboring galaxies is comparable. On the other hand, there is a relatively large difference between the fraction of Seyfert 2 and inactive galaxies possessing projected neighboring galaxies at the smallest search radius of 10 kpc, with this difference diminishing as the search radius widens until disappearing at ~ 100 kpc. Thus, the difference, if any, between the fraction of Seyfert 2 and matched samples of inactive field galaxies possessing projected neighboring galaxies depends at least in part on the search radius used. We note that this may explain the seemingly contradictory results between some optical studies; i.e., those using relatively small search radii finding a higher fraction of Seyfert with projected neighboring galaxies than in matched samples of inactive galaxies, whereas those using relatively large search radii finding no appreciable difference.

Our results agree with those of Dultzin-Hacyan et al. (1999) in two important respects. First, nearly all the Seyfert galaxies studied by Dultzin-Hacyan et al. (1999) have projected neighboring galaxies within ~ 100 kpc. Second, we both see an excess of Seyfert (our ensemble sample contains a much larger fraction of Seyfert 2 than Seyfert 1) having (projected) neighboring galaxies at projected separations smaller than ~ 90 kpc compared with the control sample. Where we differ is in our seeing this excess becoming increasingly larger with projected separation up to 90 kpc, whereas Dultzin-Hacyan et al. (1999) find this excess to become increasingly smaller with projected separation before disappearing at ~ 100 kpc. Keep in mind, however, that our HI imaging observations cleanly pick out genuine neighboring but only gas-rich galaxies, whereas those of Dultzin-Hacyan et al. (1999) may include spurious objects.

Koulouridis et al. (2006) repeated the study of Dultzin-Hacyan et al. (1999) but now armed with redshifts from the second CfA as well as Southern Sky Redshift Surveys. Confirming the trends seen by Dultzin-Hacyan et al. (1999), Koulouridis et al. (2006) find a relatively large difference between the fraction of Seyfert 2 (but, again, not Seyfert 1) with neighboring galaxies within a velocity difference of 200 km s^{-1} compared with inactive galaxies at the smallest measured projected separation of 7 kpc, with this difference diminishing as the search radius widens until disappearing at roughly 70 kpc (scaled to $H_0 = 67 \text{ km s}^{-1} \text{ Mpc}^{-1}$). With a maximum search radius of ~ 70 kpc and a limiting magnitude of $m_B \sim 15.5$ (1 magnitude brighter than the LMC at the distance of our sample), this study would have picked up only a small

fraction of the interacting neighboring galaxies that Kuo et al. (2008) detected around their Seyfert sample. Indeed, Koulouridis et al. (2006) find that only $\sim 10\%$ of Seyfert 1 and $\sim 30\%$ of Seyfert 2 galaxies have neighboring galaxies within the range of parameters searched. Going to a lower limiting magnitude of $m_B \sim 18.5$ (corresponding to the SMC at the distance of our sample) for a subset of their sample, Koulouridis et al. (2006) find that about twice as many still of both Seyfert 1 and Seyfert 2 galaxies have neighboring galaxies within a projected separation of ~ 50 kpc. This fraction is comparable to that we found in our Seyfert sample ($\sim 40\%$ at a projected separation of ~ 50 kpc). Unfortunately, Koulouridis et al. (2006) did not search for neighboring galaxies down to the same low limiting magnitudes around their control samples, and hence a more detailed comparison cannot be made.

5.3. Implicating Tidal Interactions in Triggering AGNs

The contrast between the prevalence of HI disturbances in the active and control samples is dramatic. In the active galaxy sample, we can only find a few galaxies that are not disturbed spatially and usually also kinematically on galactic-wide ($\gtrsim 20$ kpc) scales. In the control sample, we find the opposite result, with most exhibiting no detectable spatial or kinematic disturbances on both the same as well as smaller ($\gtrsim 10$ kpc) scales.

Specifically, of the eighteen galaxies in the ensemble sample of twenty-three active galaxies classified as Seyferts, seventeen ($\sim 94\%$) exhibit HI disturbances. In at least $\sim 67\%$ and possibly as high as $\sim 94\%$ of cases, the observed HI disturbances can be traced to tidal interactions with neighboring galaxies detected also in HI. By contrast, only four of the twenty-one ($\sim 19\%$) galaxies in our control sample exhibit HI disturbances. Removing the one disturbed galaxy since found to be a Seyfert 2 galaxy, only three of the twenty (15%) are actually disturbed in HI. Only one of the eighteen ($\sim 6\%$) Seyfert galaxies in the ensemble active galaxy sample exhibit no detectable HI disturbances whatsoever. By contrast, seventeen of the twenty ($\sim 85\%$) galaxies in our control sample exhibit no detectable HI disturbances. These results directly implicate tidal interactions in initiating events that lead to optically-luminous Seyfert activity in a large fraction of local disk galaxies.

6. SUMMARY AND CONCLUSIONS

The central purpose of this paper is to determine whether the high incidence of tidal interactions observed in HI gas for a sample of Seyfert galaxies reported in the companion paper by Kuo et al. (2008) is related to their AGN activity. Our strategy was to image at the same spatial resolution (~ 20 kpc) and sensitivity in HI gas a comparably large number of inactive galaxies that were closely matched in Hubble type and to the degree possible optical luminosity, as well as range in size and inclination, to the active galaxies. We detected twenty-one of the twenty-seven galaxies in our control sample, imaged at the same spatial resolution and HI column density threshold as the active galaxy sample. These twenty-one galaxies comprised our ensemble control sample from which we drew the following statistical results.

1. Only four of the twenty-one galaxies ($\sim 19\%$) exhibit spatial and usually also kinematic distur-

bances on galactic ($\gtrsim 20$ kpc) scales. One of these disturbed galaxies has since been found to be a Seyfert 2 galaxy, and so only three of the twenty (15%) inactive galaxies in our ensemble control sample are actually disturbed in HI.

2. Seventeen of the twenty-one galaxies ($\sim 81\%$) show no HI disturbances whatsoever on galactic ($\gtrsim 20$ kpc) scales. Excluding again the one disturbed galaxy since found to be a Seyfert 2 galaxy, seventeen of the twenty (85%) inactive galaxies in our ensemble control sample are not disturbed in HI.

By contrast, of the eighteen galaxies in the ensemble sample of twenty-three active galaxies classified as Seyferts, seventeen ($\sim 94\%$) exhibit HI disturbances. In at least $\sim 67\%$ and possibly as high as $\sim 94\%$ of cases, the observed HI disturbances can be traced to tidal interactions with neighboring galaxies detected also in HI. The dramatic contrast in the incidence of HI disturbances between the active and inactive galaxy samples strongly implicates tidal interactions in initiating events that lead to luminous Seyfert activity in a large fraction of local disk galaxies.

Acknowledgements

Jenny Greene was largely responsible for selecting the control sample. We thank A.-L. Tsai and S.-Y. Lin for reducing part of the data. We thank the important comments from the referee. The National Radio Astronomy Observatory is a facility of the National Science Foundation operated under cooperative agreement by Associated Universities, Inc. Y.-W. Tang, C.-Y. Kuo, A.-L. Tsai, and S.-Y. Lin all acknowledge the support of a Research Assistantship at the ASIAA where the bulk of this work was done. J. Lim acknowledges the National Science Council of Taiwan for providing a grant in support of this work. This research has made use of NASA's Astrophysics Data System Bibliographic Services, and the NASA/IPAC Extragalactic Database (NED) which is operated by the Jet Propulsion Laboratory, California Institute of Technology, under contract with the National Aeronautics and Space Administration. We acknowledge the usage of the HyperLeda database (<http://leda.univ-lyon1.fr>).

REFERENCES

- Condon, J. J., Cotton, W. D., Greisen, E. W., Yin, Q. F., Perley, R. A., Taylor, G. B., & Broderick, J. J., AJ, 115, 1693
- Dahari, O. 1984, AJ, 89, 966
- de Robertis, M. M., Hayhoe, K., & Yee, H. K. C. 1998a, ApJ, 115, 163
- de Robertis, M. M., Yee, H. K. C., & Hayhoe, K. 1998b, ApJ, 496, 93
- Dultzin-Hacyan, D., Krongold, Y., Fuentes-Guridi, I., & Marziani, P. 1999, ApJ, 513, 111
- Fuentes-Williams, T. & Stocke, J. T. 1988, AJ, 96, 1235
- Giovanelli, R. & Haynes, M. 1981, AJ, 86, 340
- Huchra, J., Davis, M., Latham, D., & Tonry, J. 1983, ApJS, 52, 89
- Huchra, J. P., Geller, M. J., & Corwin, H. G. Jr. 1995, ApJS, 99, 391
- Huchtmeier, W. K. & Richter, O.-G. 1989, A General Catalog of H I Observations of Galaxies (Berlin: Springer)
- Iono, D., Yun, M. S., & Ho, P.T.P. 2005, ApJS, 158, 1
- Koulouridis, E., Plionis, M., Chavushyan, V., Dultzin-Hacyan, D., Krongold, Y., & Goudis, C. 2006, ApJ, 639, 37
- Kuo, C.-Y., Lim, J., Tang, Y.-W., & Ho, P. T. P. 2008, submitted
- Lipovetsky, V. A., Neizvestny, S. I., & Neizvestnaya, O. M. 1988, Soob. Spets. Astrofiz. Obs., 55, 5
- MacKenty, J. W. 1989, ApJ, 343, 125
- Martini, P. 2004, in IAU Symp. 222, The Interplay among Black Holes, Stars and ISM in Galactic Nuclei, ed. Th. S. Bergmann, L. C. Ho, & H. R. Schmitt (San Francisco: ASP), 557
- Paturel, G., Petit, C., Prugniel, Ph., Theureau, G., Rousseau, J., Brouty, M., Dubois, P., & Cambrésy, L. 2003, A&A, 412, 45
- Rafanelli, P., Violato, M., & Baruffolo, A. 1995, AJ, 109, 1546
- Schmitt, H. R. 2001, AJ, 122, 2243
- Stauffer, J. R. 1982, ApJ, 262, 66
- Véron-Cetty, M.-P. & Véron, P. 1998, A Catalogue of Quasars and Active Nuclei (8th ed.; Garching: ESO)
- Véron-Cetty, M.-P. & Véron, P. 1998, A Catalogue of Quasars and Active Nuclei (9th ed.; Garching: ESO)
- Véron-Cetty, M.-P. & Véron, P. 2006, A&A, 455, 773
- Yun, M. S., Ho, P. T. P., & Lo, K. Y. 1994, Nature, 372, 530

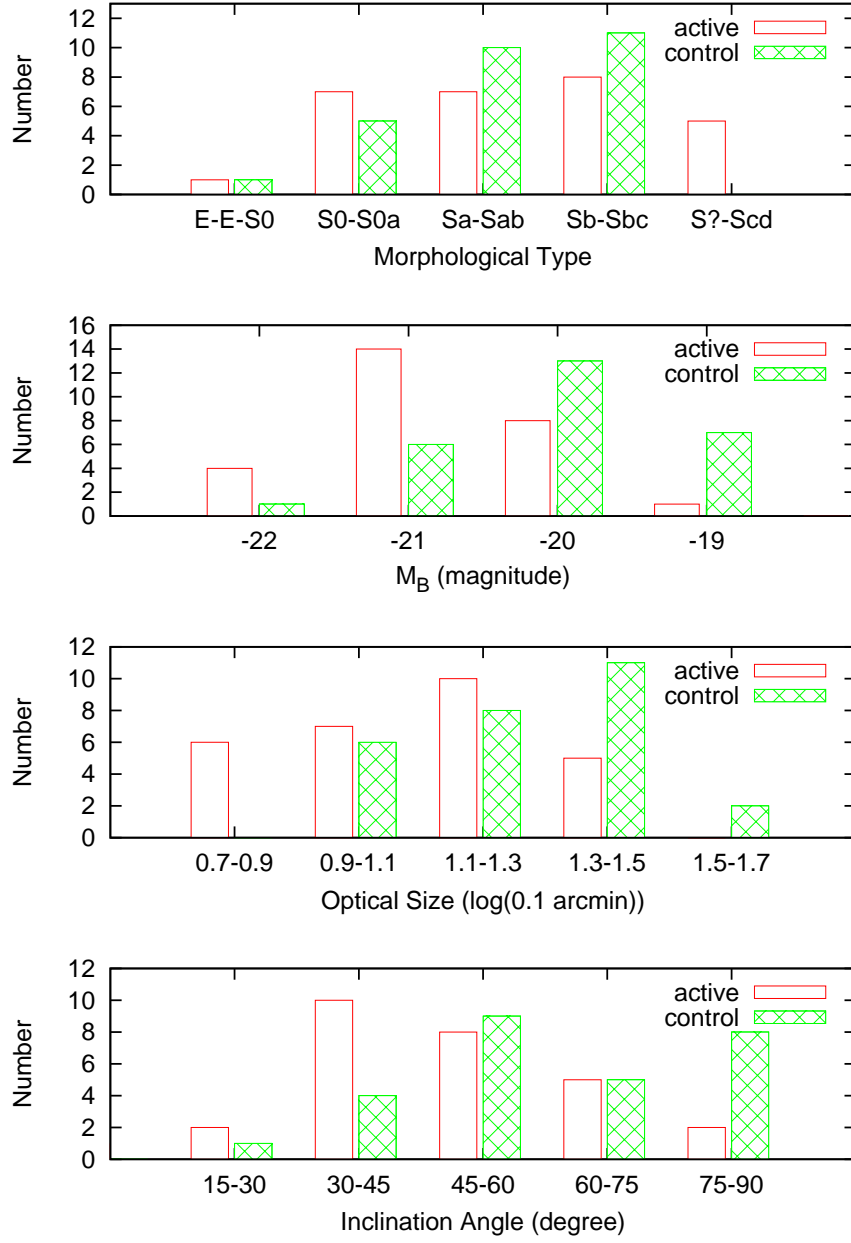


FIG. 1.— Number distribution of the active galaxy sample selected by (Kuo et al., 2008) (unfilled histogram) and the inactive control sample selected here (hatched histogram) in morphological type (upper panel), corrected absolute B-band magnitude (second panel from top, M_B), optical size (second panel from bottom), and inclination (bottom panel). The morphological type, M_B , optical size and inclination angle are retrieved from the HYPERLEDA database. Note that there are 27 active samples included in the M_B plot. The M_B of MS 04595+0327 is not available in the HYPERLEDA database. The rest of the plots include all the sample.

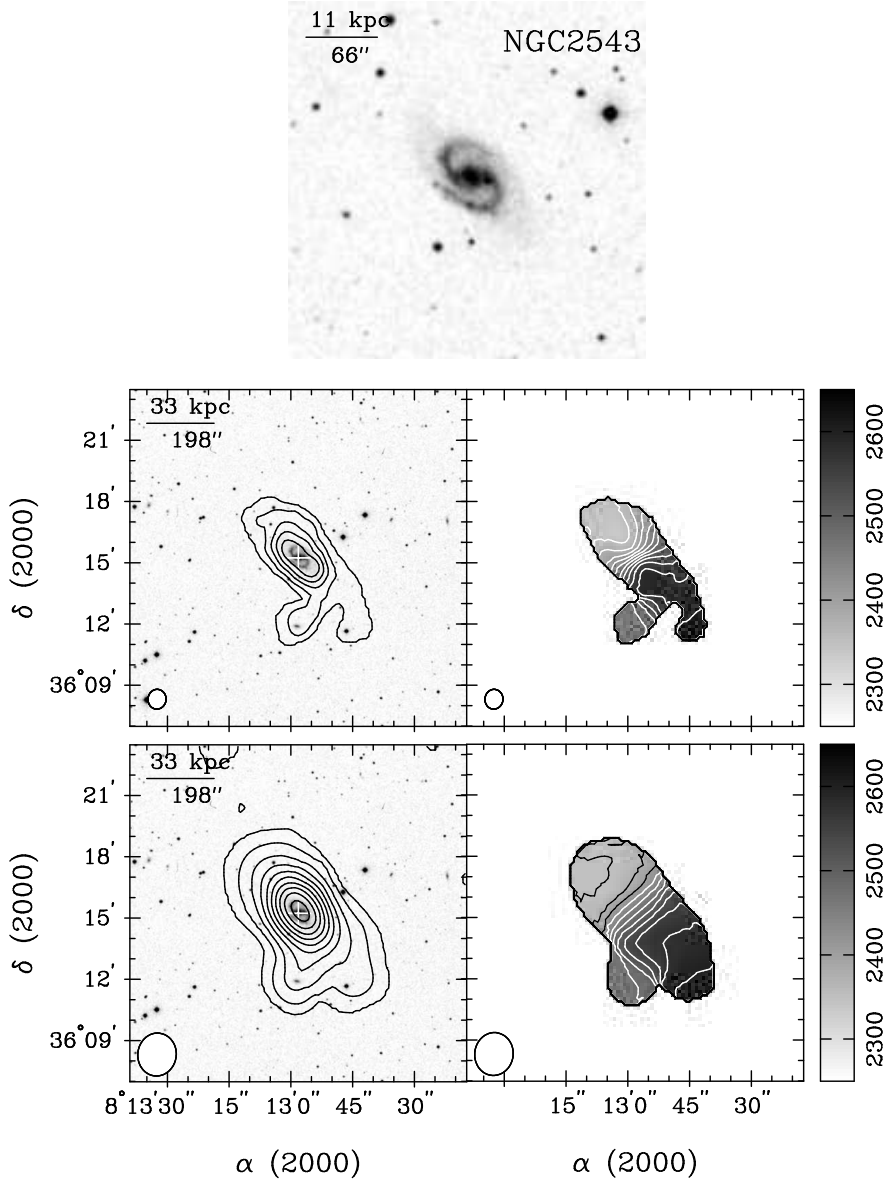


FIG. 2.— Upper panel: Optical image of NGC 2543 (Control sample) from the Second Digitized Sky Survey (DSS2). Middle panels: (Left) Contours of integrated HI intensity (zeroth moment) overlaid on the DSS2 image, and (Right) map of intensity-weighted HI mean velocity (first moment) with full resolution. Lower panels: (Left) Contours of zeroth moment overlaid on the DSS2 image and (Right) first moment map with the same spatial resolution as the Seyfert sample. In the zeroth moment maps with full resolution, contours are plotted at $3, 20, 40, 60, 80 \times 20.0 \text{ mJy beam}^{-1} \text{ km s}^{-1}$ ($1.0 \times 10^{19} \text{ cm}^{-2}$). In the zeroth moment maps with the same spatial resolution as the Seyfert sample, contours are plotted at $3, 20, 40, 60, 80 \times 28.3 \text{ mJy beam}^{-1} \text{ km s}^{-1}$ ($3.2 \times 10^{18} \text{ cm}^{-2}$). In the first moment map, heliocentric velocities are indicated by the scale wedge (in km/s), and contours plotted at intervals of 25 km s^{-1} . The ellipse at the lower left corner of the lower panels is the half-power width of the synthesized beam, and has a size of $58'' \times 53''$ (full resolution) and $126'' \times 113''$ (the same spatial resolution as the Seyfert sample).

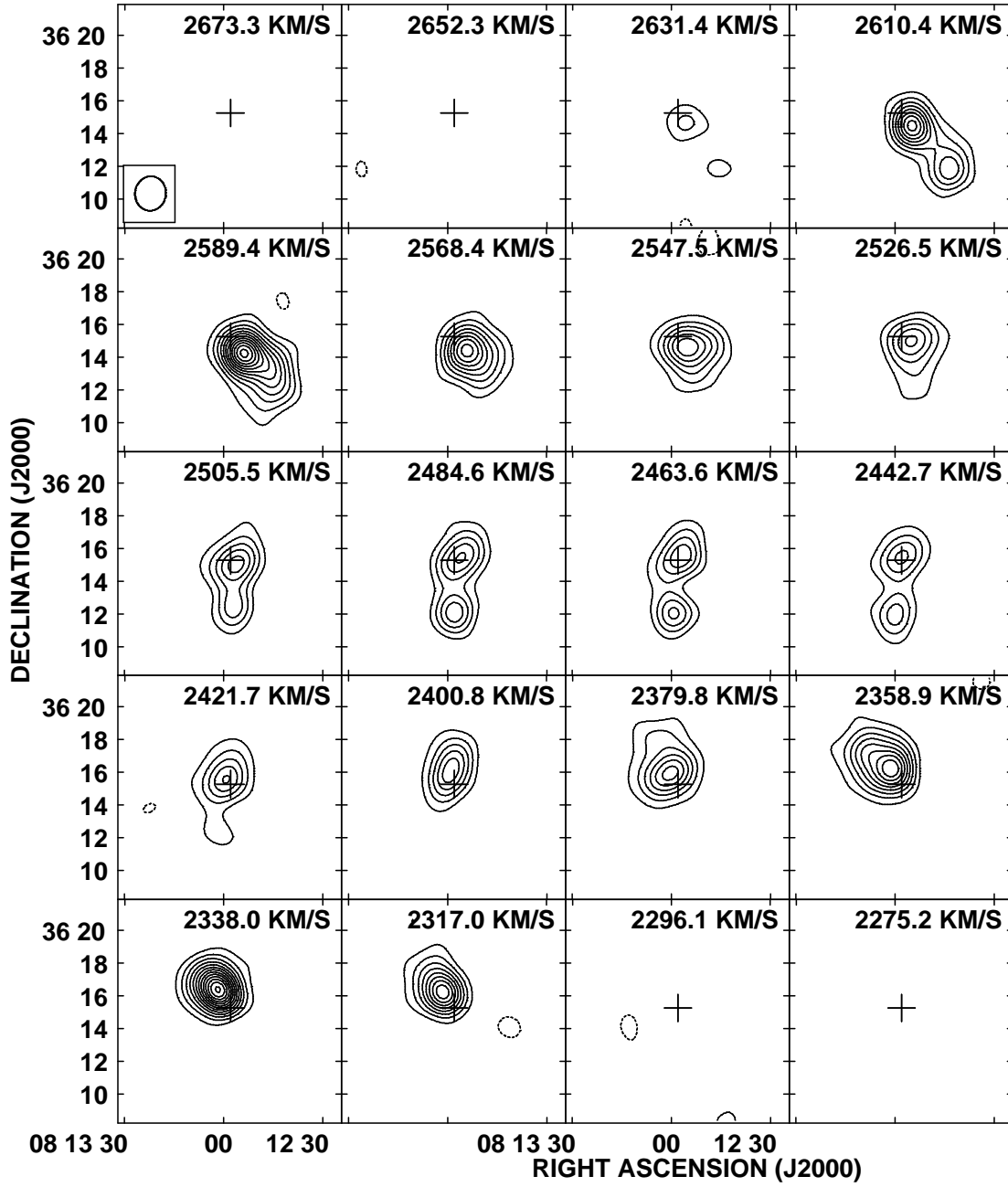


FIG. 3.— HI channel maps of NGC 2543 with spatial resolution the same as the Seyfert sample. Contour levels are plotted at $-3, 3, 6, 9, 12, 15, 18 \times 0.18 \text{ mJy beam}^{-1}$ (1σ), which corresponds to a HI column density of $2.0 \times 10^{16} \text{ cm}^{-2}$. The central heliocentric velocity is shown for each channel. The cross marks the position of NGC 2543. The synthesized beam is shown by the ellipse at the lower left corner of the top left panel.

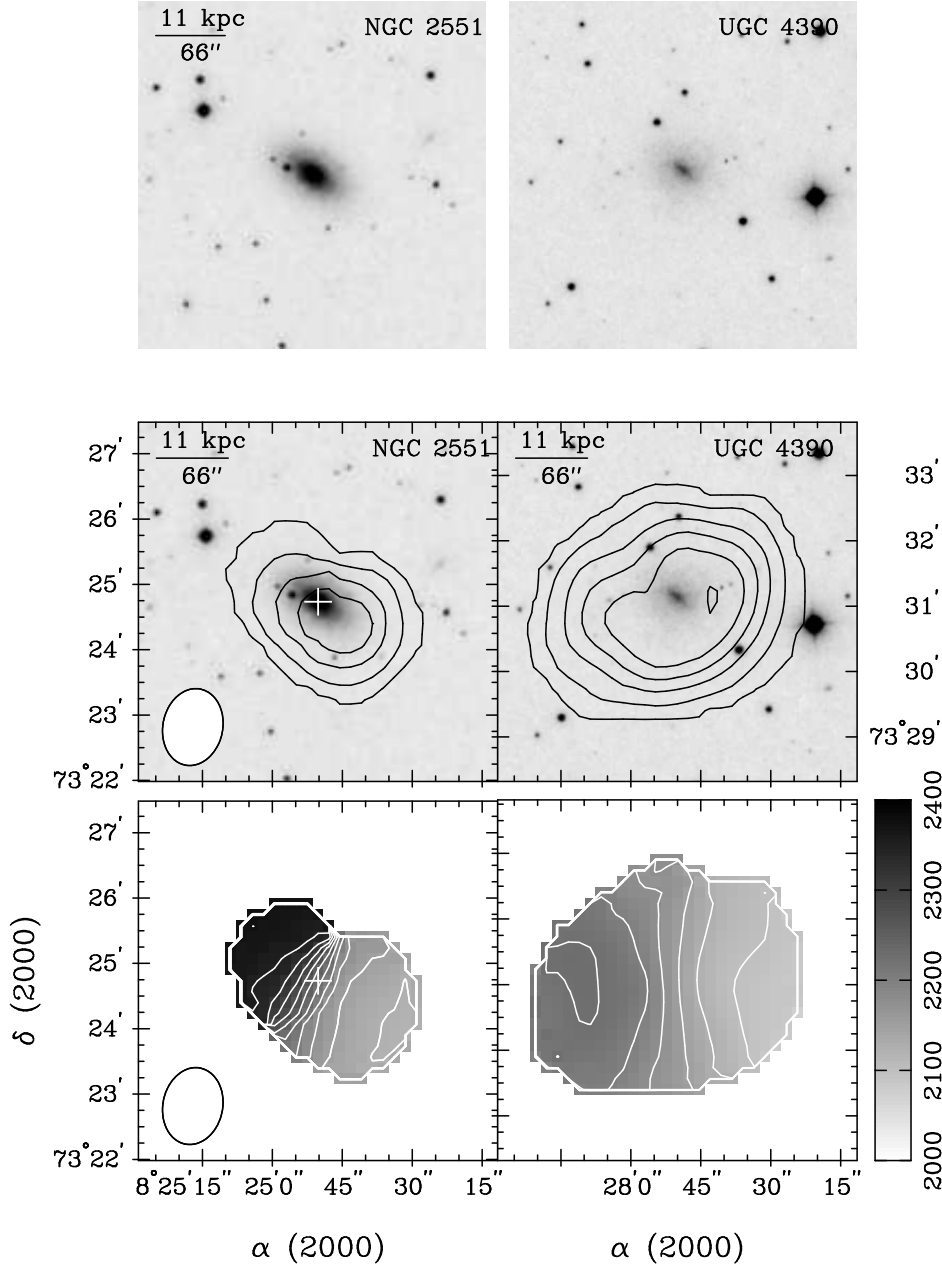


FIG. 4.— Upper panels: Optical images of (*Left*) NGC 2551 (Control sample) and (*Right*) UGC 4390 from DSS2. Middle panels: Contours of zeroth moment overlaid on the DSS2 images. Lower panels: First moment maps. In the zeroth moment map, contours are plotted at 3, 10, 20, 30, 40 (NGC 2551) and 3, 6, 9, 12, 15, 18 (UGC 4390) $\times 24.0 \text{ mJy beam}^{-1} \text{ km s}^{-1}$ ($9.8 \times 10^{18} \text{ cm}^{-2}$). The half-power width of the synthesized beam has a size of $72'' \times 55''$.

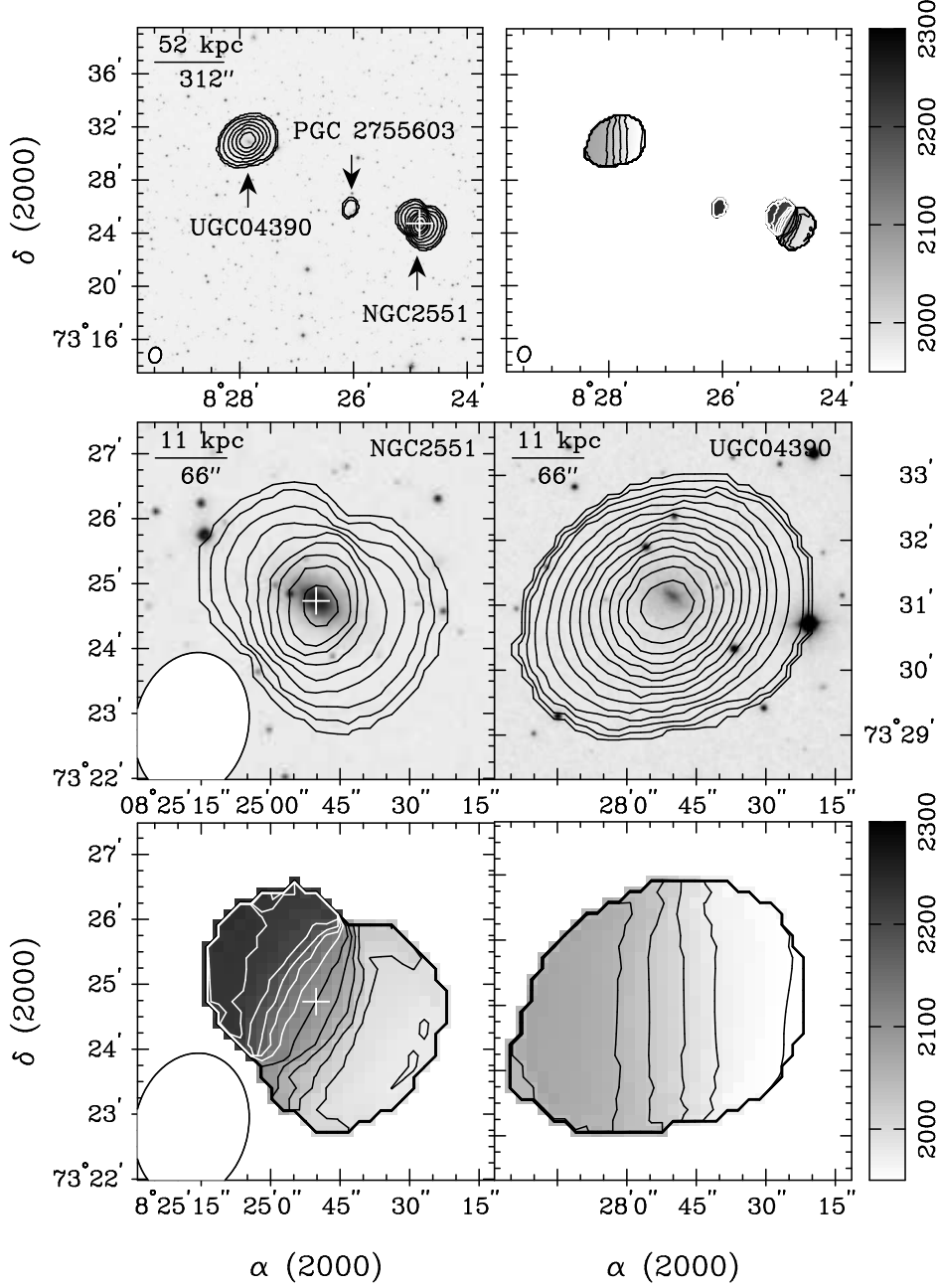


FIG. 5.— Upper panels: (Left) Contours of zeroth moment of NGC 2551 and UGC 4390 overlaid on the DSS2 image and (Right) first moment map with larger field. Middle panels: Contours of zeroth moment with the same spatial resolution as the Seyfert sample overlaid on the DSS2 images. Lower panels: First moment maps with the same spatial resolution as the Seyfert sample. In the zeroth moment maps, contours are plotted at 3, 20, 40, 60, 80 $\times 24.0$ mJy beam $^{-1}$ km s $^{-1}$ (9.8×10^{18} cm $^{-2}$). The half-power width of the synthesized beam has a size of $136'' \times 105''$.

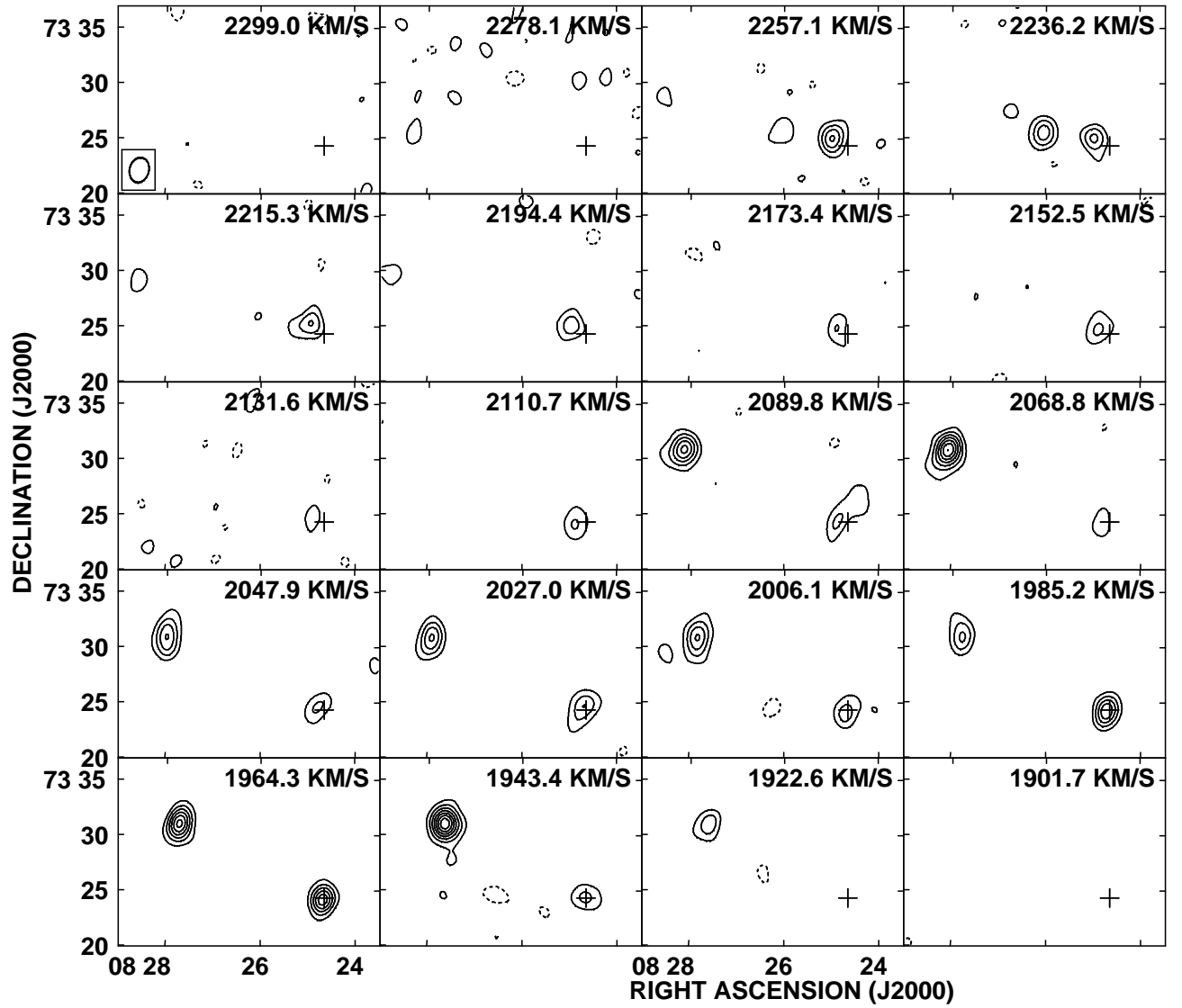


FIG. 6.— HI channel maps of NGC 2551 with spatial resolution the same as the Seyfert sample. Contour levels are plotted at $-3, 3, 6, 9, 12, 15, 18 \times 0.18 \text{ mJy beam}^{-1}$ (1σ), which corresponds to a HI column density of $2.0 \times 10^{16} \text{ cm}^{-2}$. The cross marks the position of NGC 2551.

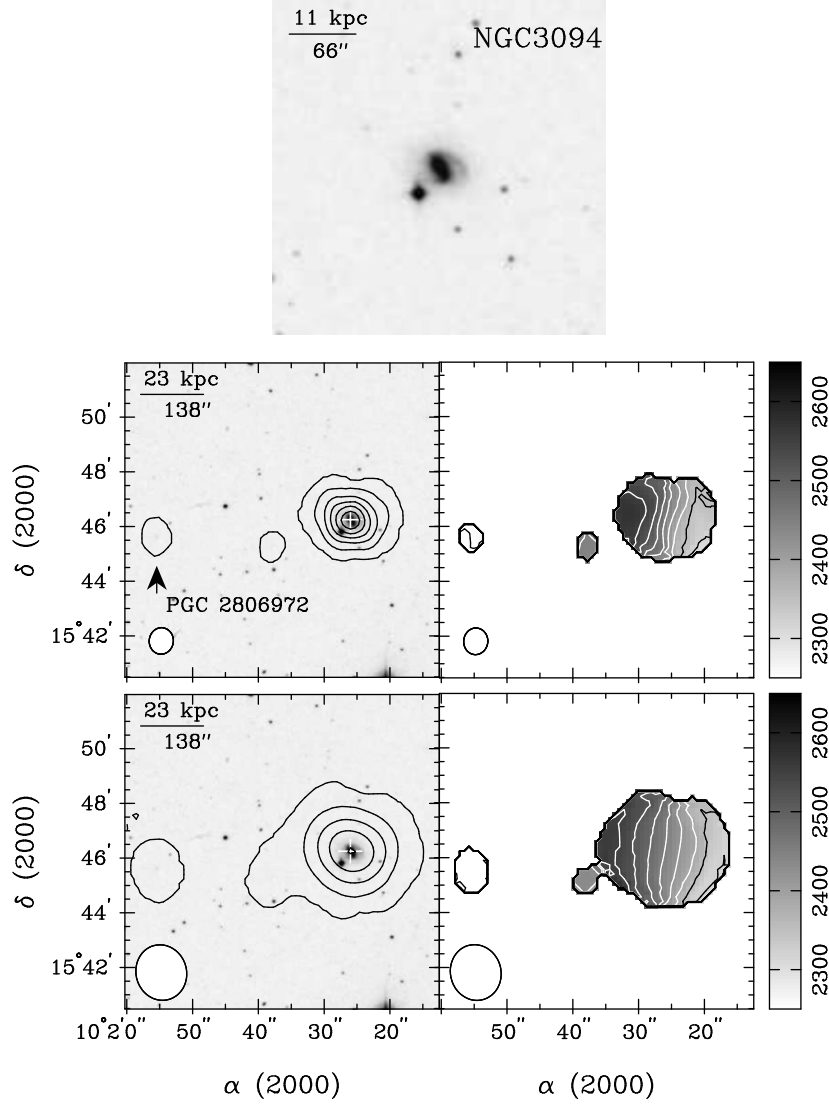


FIG. 7.— Upper panel: Optical images of NGC 3094 (Control sample) from DSS2. Middle panels: (*Left*) Contours of zeroth moment overlaid on the DSS2 image and (*Right*) first moment map with full resolution. Lower panels: (*Left*) Contours of zeroth moment and (*Right*) first moment map with the same spatial resolution as the Seyfert sample. In the zeroth moment maps with full resolution, contours are plotted at 3, 20, 40, 60, 80 \times 28.2 mJy beam $^{-1}$ km s $^{-1}$ (1.5×10^{19} cm $^{-2}$). In the zeroth moment maps with the same spatial resolution as the Seyfert sample, contours are plotted at 3, 20, 40, 60, 80 \times 71.7 mJy beam $^{-1}$ km s $^{-1}$ (8.5×10^{18} cm $^{-2}$). The half-power width of the synthesized beam has a size of 59'' \times 52'' (full resolution) and 123'' \times 111'' (the same spatial resolution as the Seyfert sample).

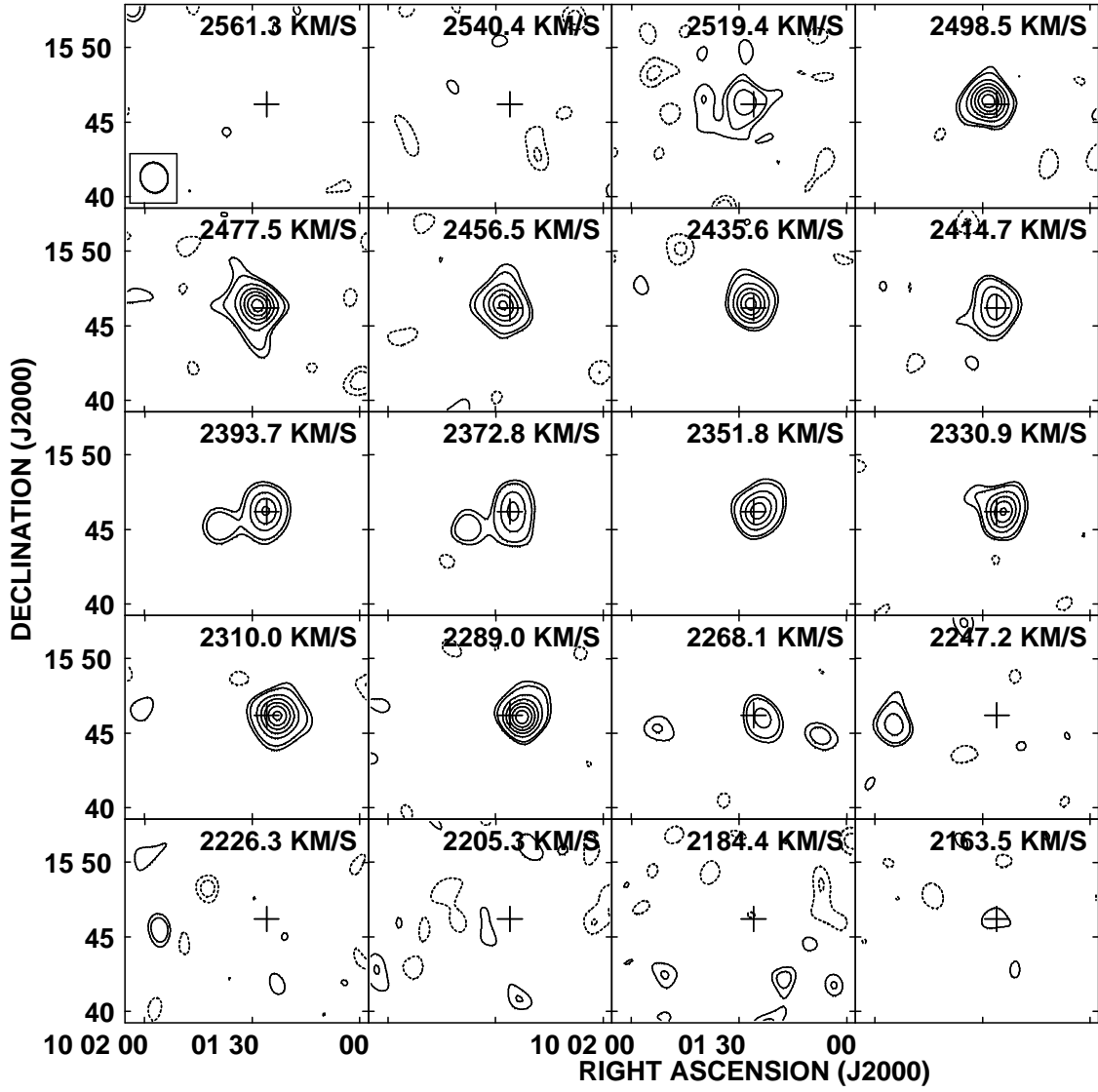


FIG. 8.— HI channel maps of NGC 3094 with spatial resolution the same as the Seyfert sample. Contour levels are plotted at $-3, -2, 2, 3, 6, 9, 12, 15 \times 0.18 \text{ mJy beam}^{-1}$ (1σ), which corresponds to a HI column density of $2.0 \times 10^{16} \text{ cm}^{-2}$. The cross marks the position of NGC 3094.

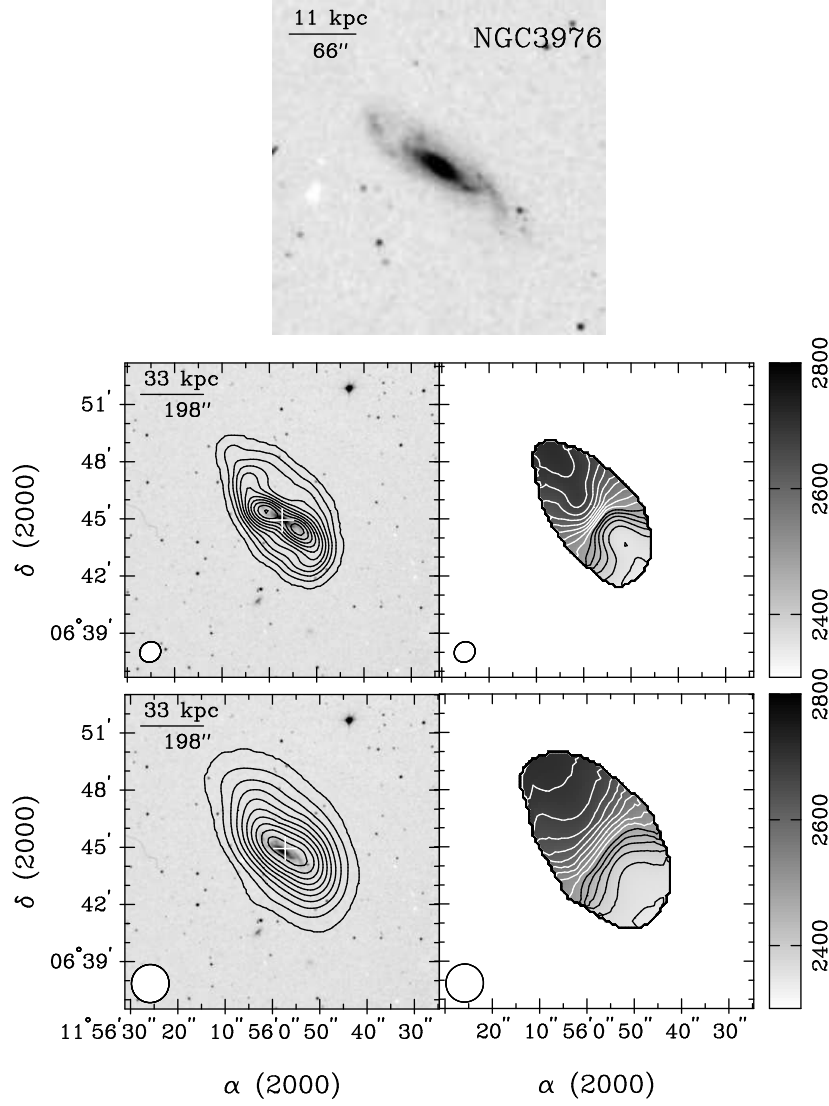


FIG. 9.— Upper panel: Optical images of NGC 3976 (Control sample) from DSS2. Middle panels: (*Left*) Contours of zeroth moment overlaid on the DSS2 image and (*Right*) first moment map with full resolution. Lower panels: (*Left*) Contours of zeroth moment and (*Right*) first moment map with the same spatial resolution as the Seyfert sample. In the zeroth moment maps with full resolution, contours are plotted at 3, 20, 40, 60, $80 \times 28.2 \text{ mJy beam}^{-1} \text{ km s}^{-1}$ ($1.1 \times 10^{19} \text{ cm}^{-2}$). In the zeroth moment maps with the same spatial resolution as the Seyfert sample, contours are plotted at 3, 20, 40, 60, $80 \times 71.2 \text{ mJy beam}^{-1} \text{ km s}^{-1}$ ($8.1 \times 10^{18} \text{ cm}^{-2}$). The half-power width of the synthesized beam has a size of $68'' \times 62''$ (full resolution) and $120'' \times 118''$ (the same spatial resolution as the Seyfert sample).

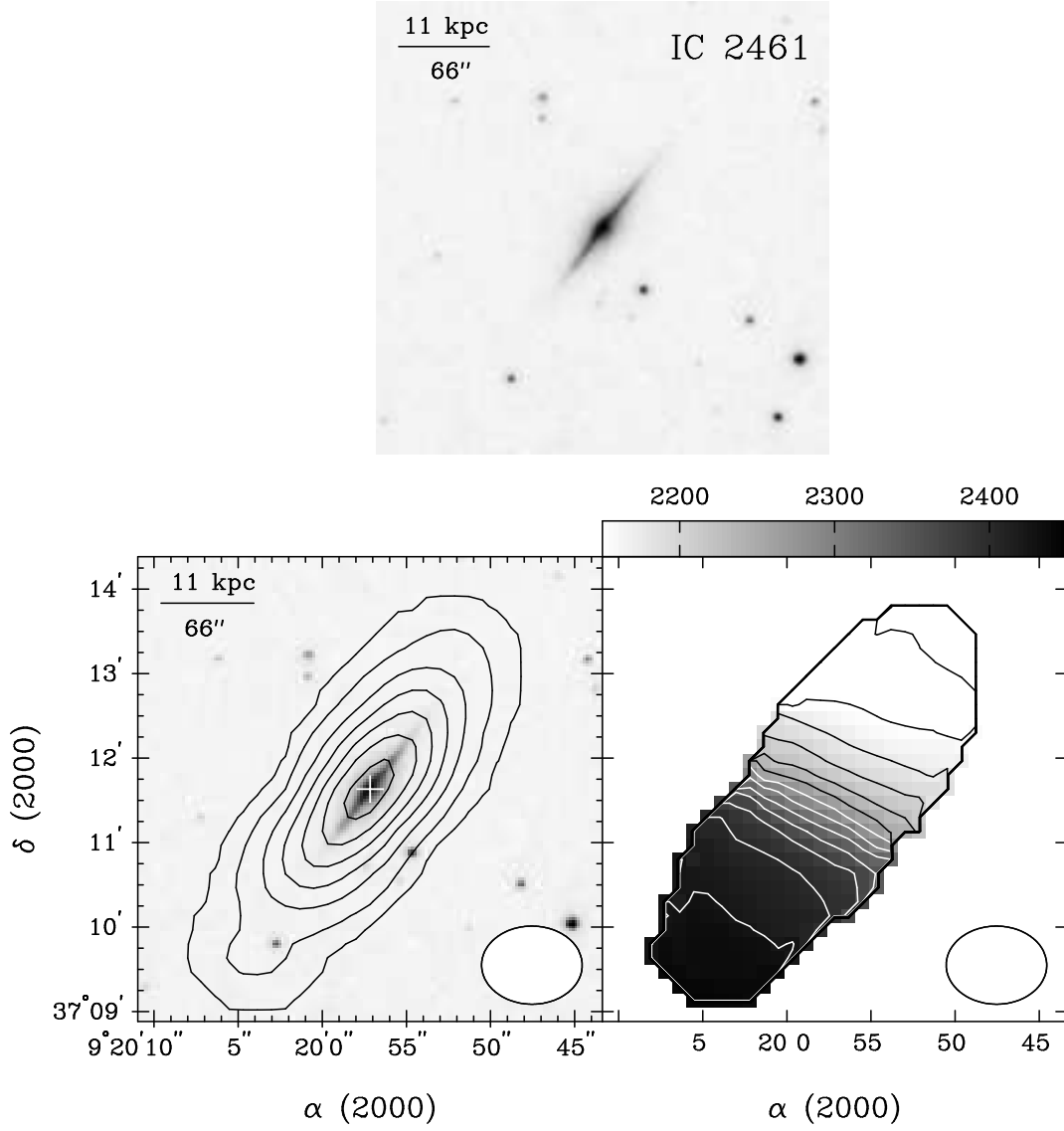


FIG. 10.— Upper panel: Optical image of IC 2461 (Control sample) from the DSS2. Lower panels: (*Left*) Contours of zeroth moment overlaid on the DSS2 image, and (*Right*) first moment map. In the zeroth moment map, contours are plotted at 3, 20, 40, 60, 80 \times 26.8 mJy beam $^{-1}$ km s $^{-1}$ (1.1×10^{19} cm $^{-2}$). The half-power width of the synthesized beam has a size of 72" \times 55".

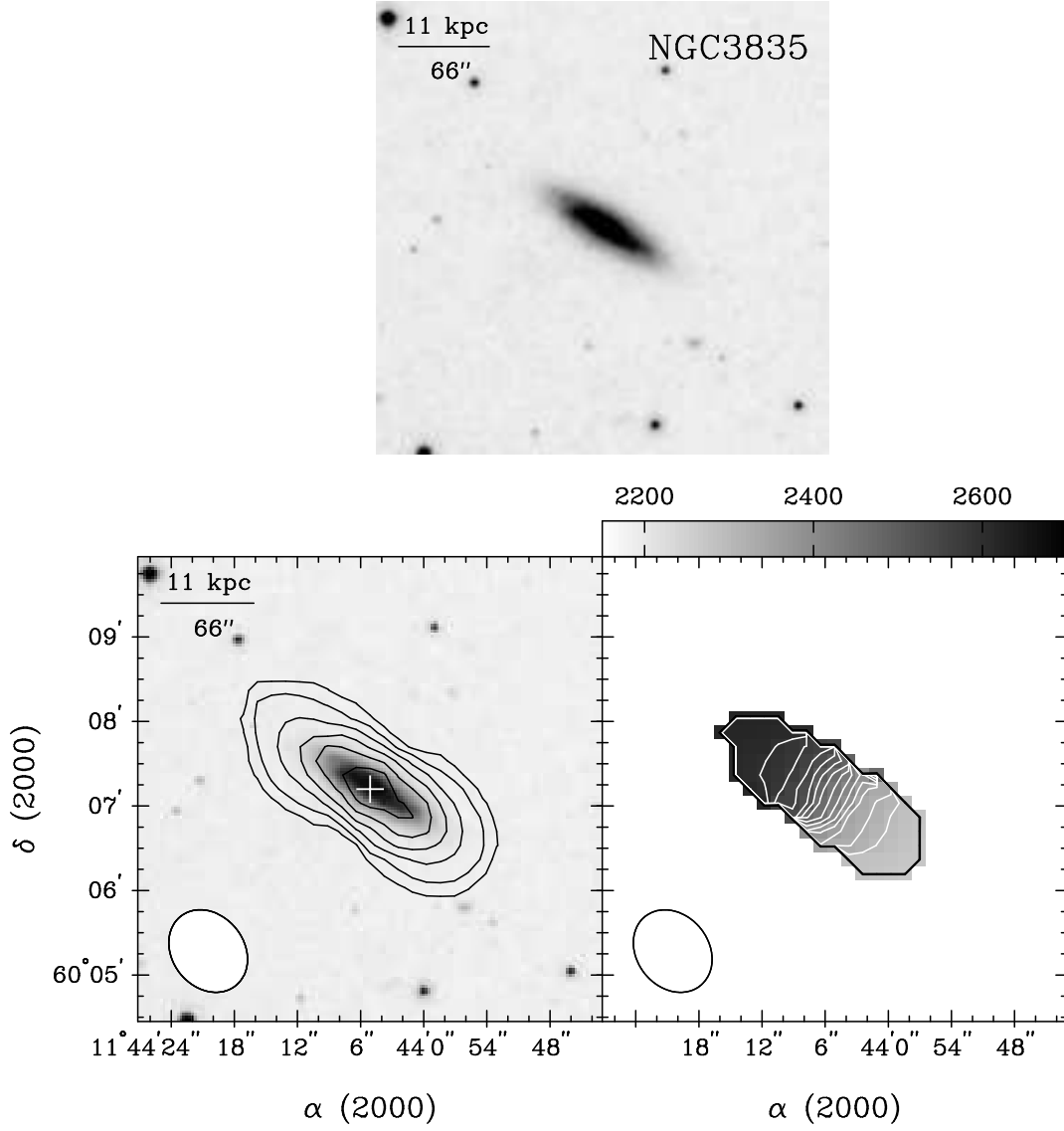


FIG. 11.— Upper panel: Optical image of NGC 3835 (Control sample) from the DSS2. Lower panels: (*Left*) Contours of zeroth moment overlaid on the DSS2 image, and (*Right*) first moment map. In the zeroth moment map, contours are plotted at 3, 10, 20, 30, $40 \times 31.2 \text{ mJy beam}^{-1} \text{ km s}^{-1}$ ($1.6 \times 10^{19} \text{ cm}^{-2}$). The half-power width of the synthesized beam has a size of $63'' \times 51''$.

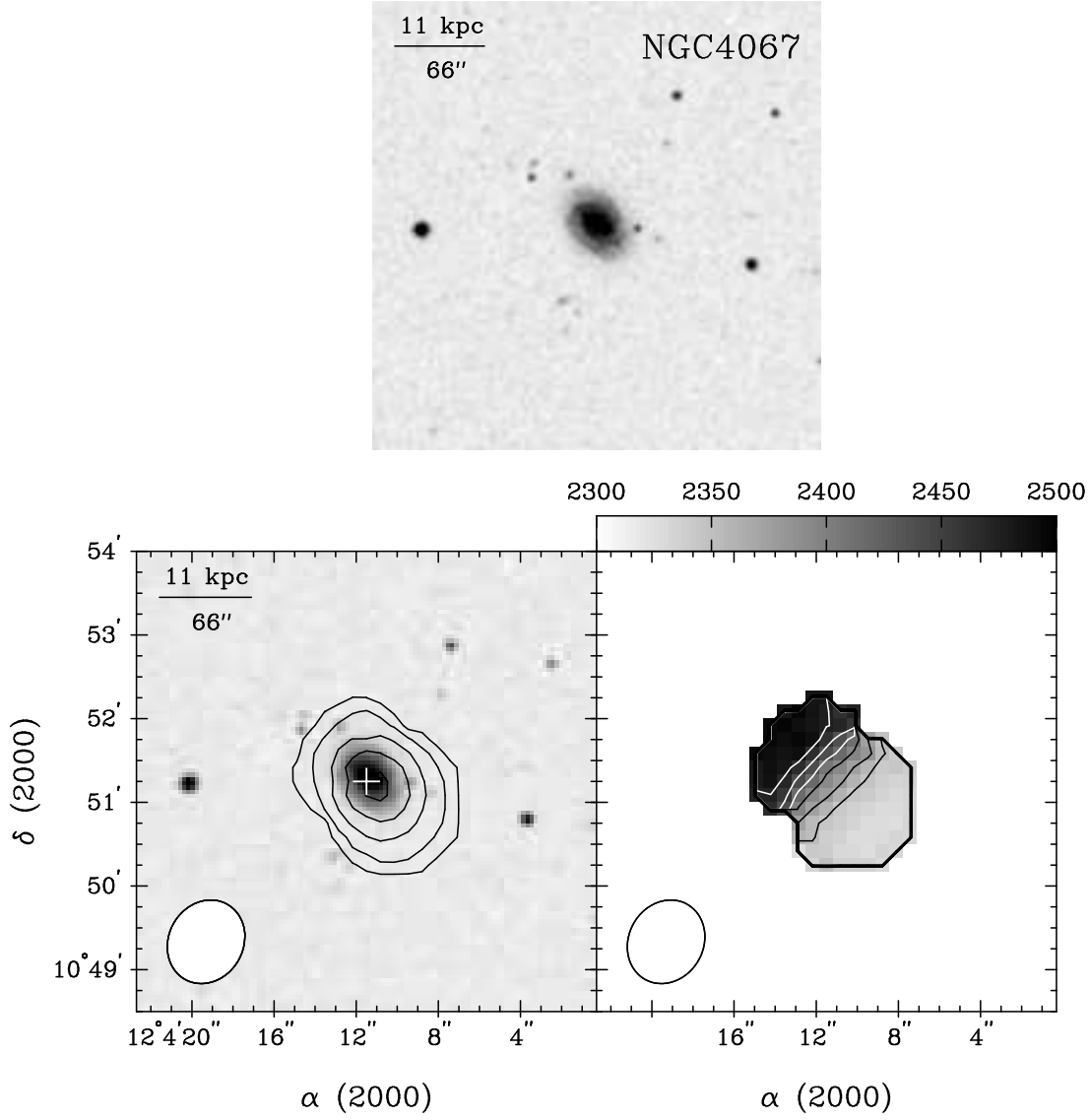


FIG. 12.— Upper panel: Optical image of NGC 4067 (Control sample) from the DSS2. Lower panels: (*Left*) Contours of zeroth moment overlaid on the DSS2 image, and (*Right*) first moment map. In the zeroth moment map, contours are plotted at 3, 10, 20, 30, $40 \times 31.2 \text{ mJy beam}^{-1} \text{ km s}^{-1}$ ($1.5 \times 10^{19} \text{ cm}^{-2}$). The half-power width of the synthesized beam has a size of $62'' \times 54''$.

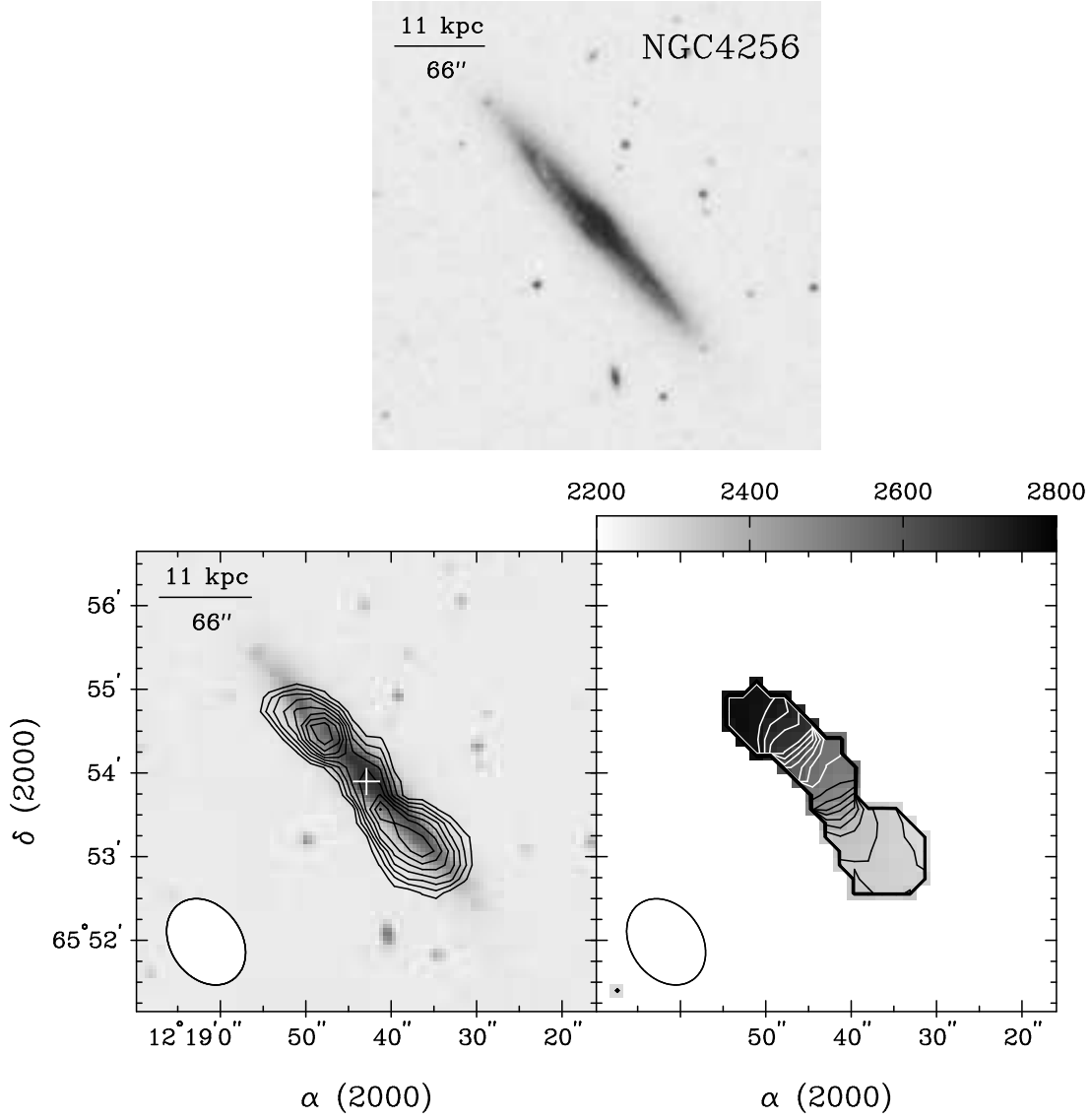


FIG. 13.— Upper panel: Optical image of NGC 4256 (Control sample) from the DSS2. Lower panels: (*Left*) Contours of zeroth moment overlaid on the DSS2 image, and (*Right*) first moment map. In the zeroth moment map, contours are plotted at 3, 6, 9, 12, $15 \times 38.0 \text{ mJy beam}^{-1} \text{ km s}^{-1}$ ($1.8 \times 10^{19} \text{ cm}^{-2}$). The half-power width of the synthesized beam has a size of $67'' \times 51''$.

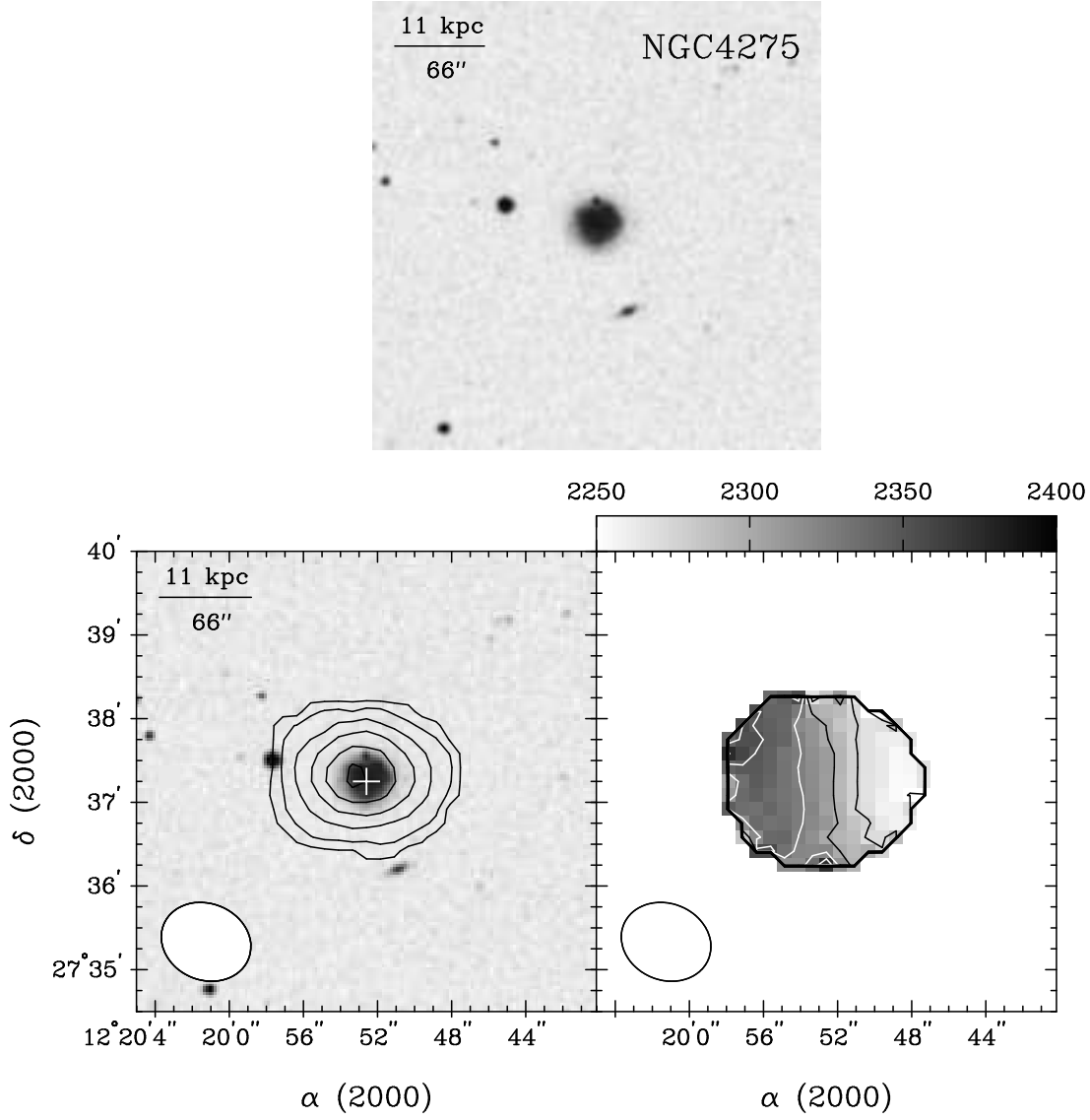


FIG. 14.— Upper panel: Optical image of NGC 4275 (Control sample) from the DSS2. Lower panels: (*Left*) Contours of zeroth moment overlaid on the DSS2 image, and (*Right*) first moment map. In the zeroth moment map, contours are plotted at 3, 10, 20, 30, $40 \times 23.2 \text{ mJy beam}^{-1} \text{ km s}^{-1}$ ($1.1 \times 10^{19} \text{ cm}^{-2}$). The half-power width of the synthesized beam has a size of $63'' \times 55''$.

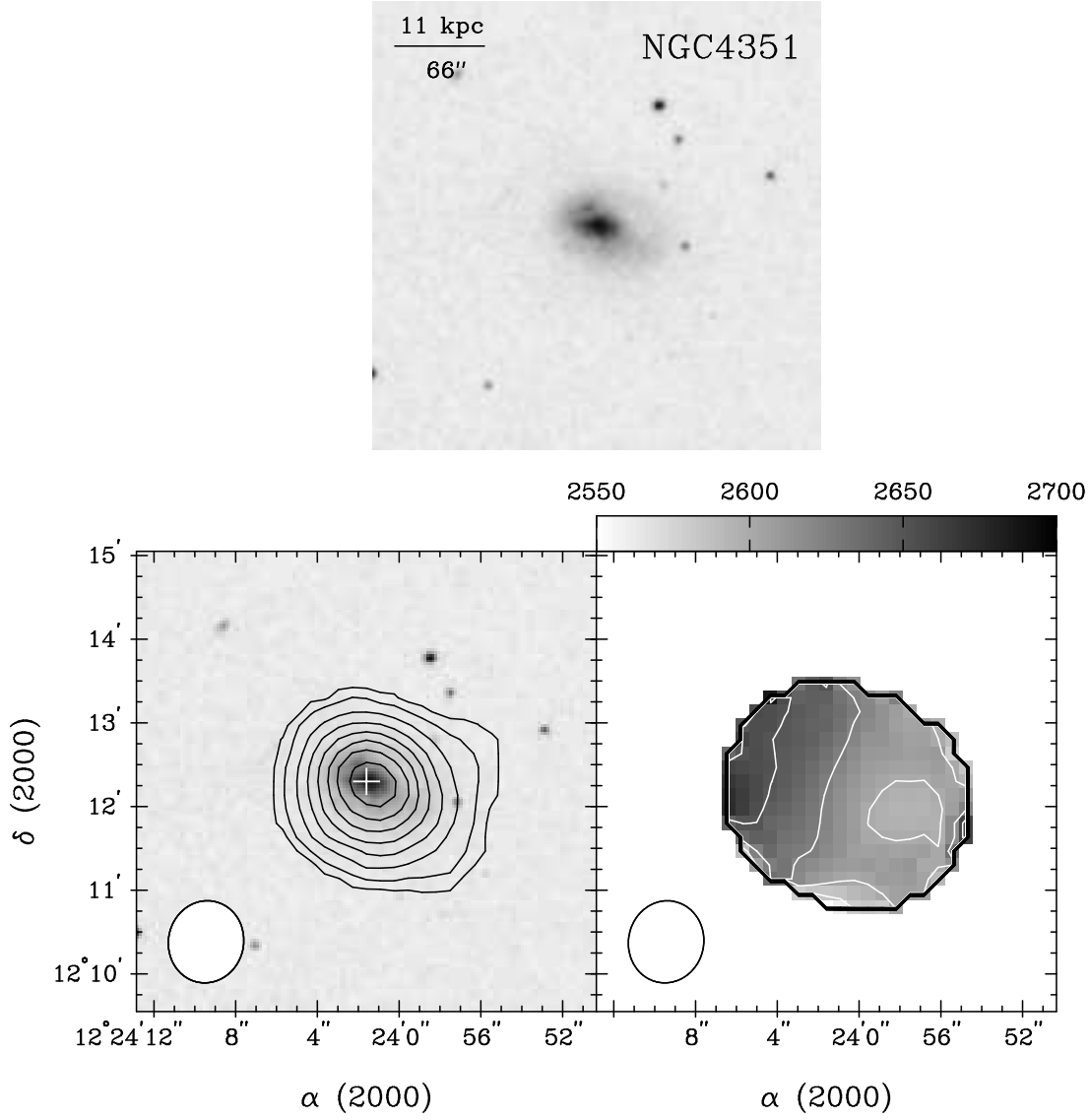


FIG. 15.— Upper panel: Optical image of NGC 4351 (Control sample) from the DSS2. Lower panels: (*Left*) Contours of zeroth moment overlaid on the DSS2 image, and (*Right*) first moment map. In the zeroth moment map, contours are plotted at 3, 10, 20, 30, $40 \times 20.8 \text{ mJy beam}^{-1} \text{ km s}^{-1}$ ($1.1 \times 10^{19} \text{ cm}^{-2}$). The half-power width of the synthesized beam has a size of $59'' \times 54''$.

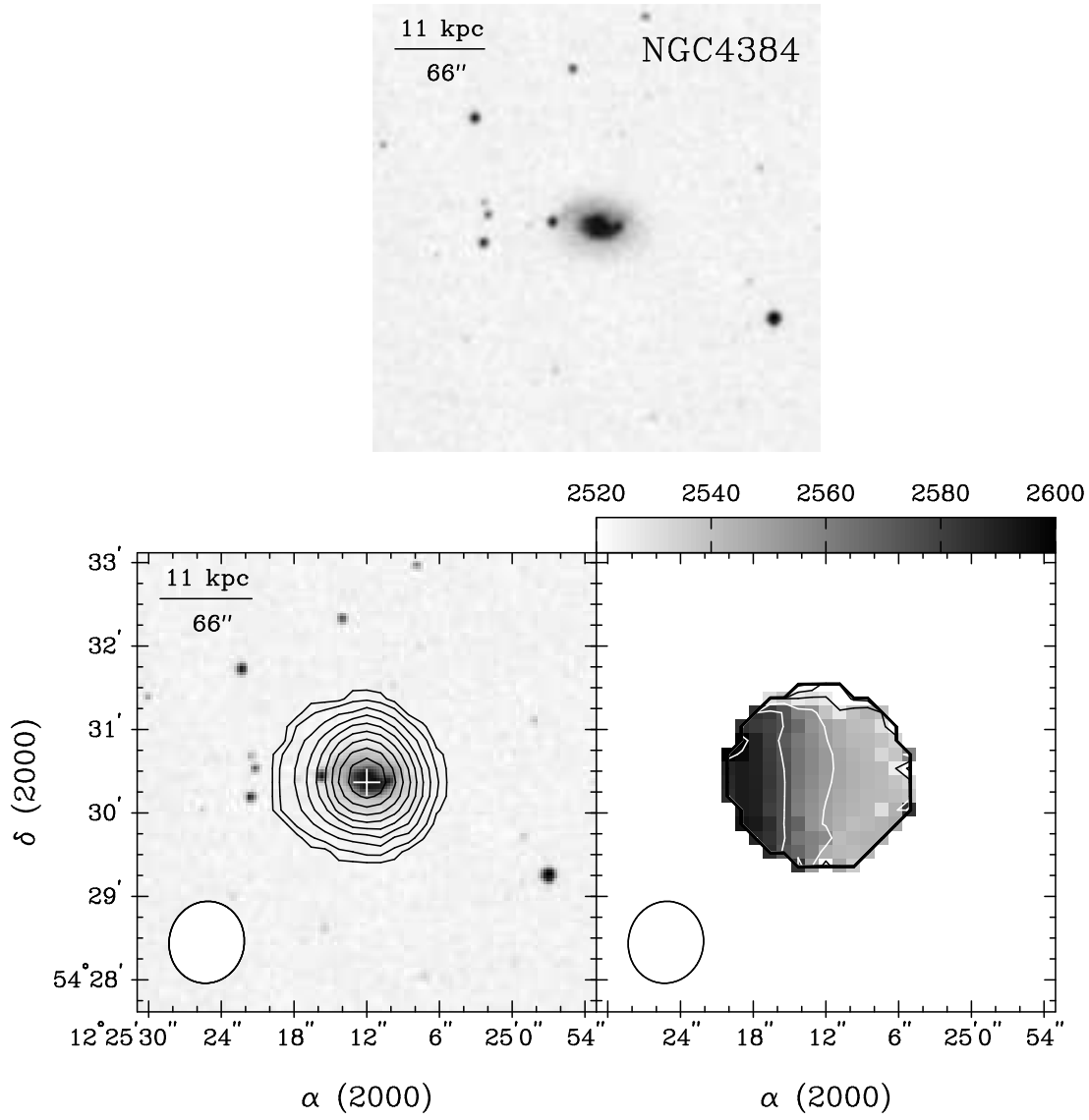


FIG. 16.— Upper panel: Optical image of NGC 4384 (Control sample) from the DSS2. Lower panels: (*Left*) Contours of zeroth moment overlaid on the DSS2 image, and (*Right*) first moment map. In the zeroth moment map, contours are plotted at 3, 10, 20, 30, $40 \times 18.0 \text{ mJy beam}^{-1} \text{ km s}^{-1}$ ($7.8 \times 10^{18} \text{ cm}^{-2}$). The half-power width of the synthesized beam has a size of $66'' \times 56''$.

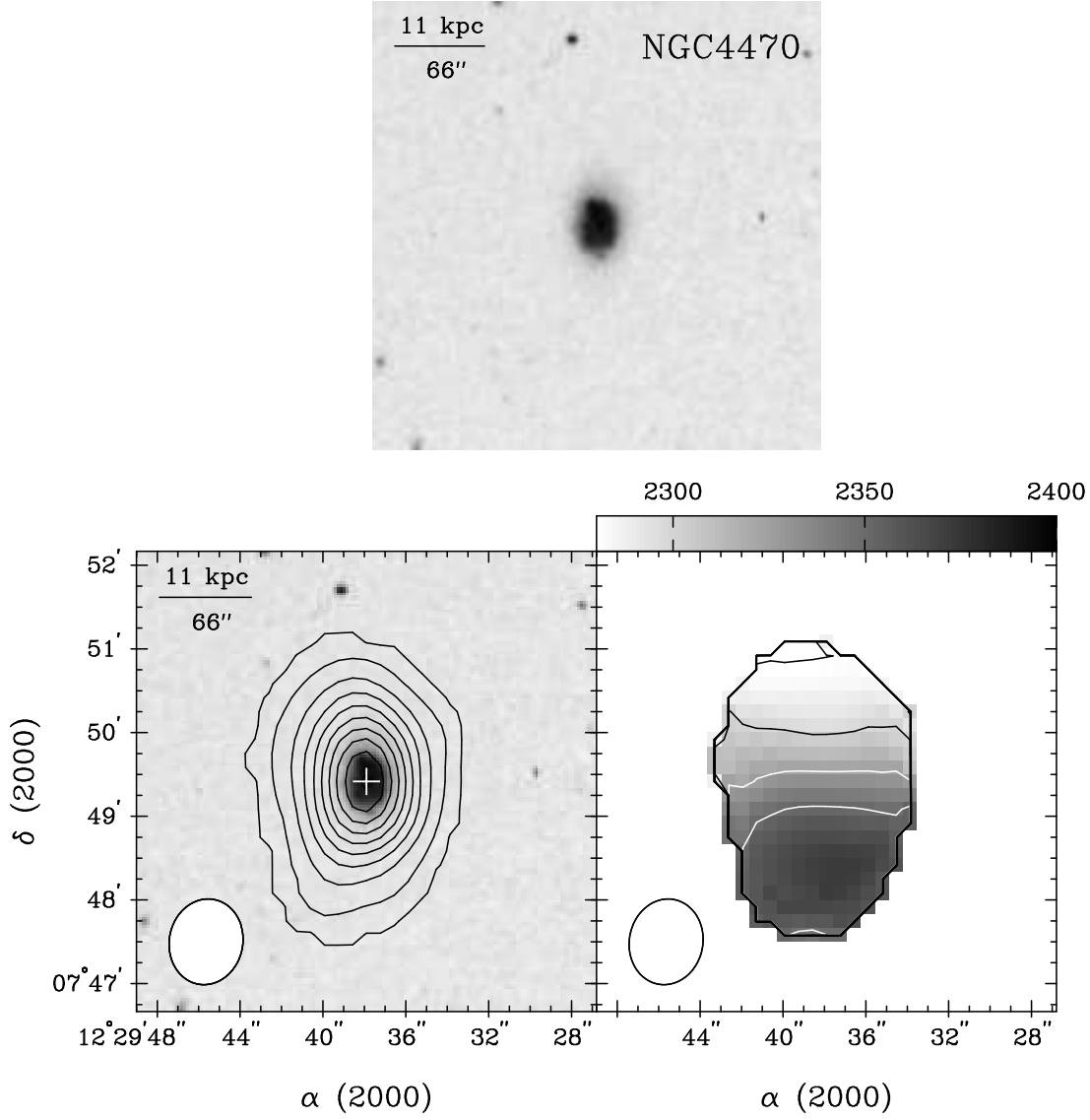


FIG. 17.— Upper panel: Optical image of NGC 4470 (Control sample) from the DSS2. Lower panels: (*Left*) Contours of zeroth moment overlaid on the DSS2 image, and (*Right*) first moment map. In the zeroth moment map, contours are plotted at 3, 20, 40, 60, $80 \times 17.0 \text{ mJy beam}^{-1} \text{ km s}^{-1}$ ($8.4 \times 10^{18} \text{ cm}^{-2}$). The half-power width of the synthesized beam has a size of $62'' \times 53''$.

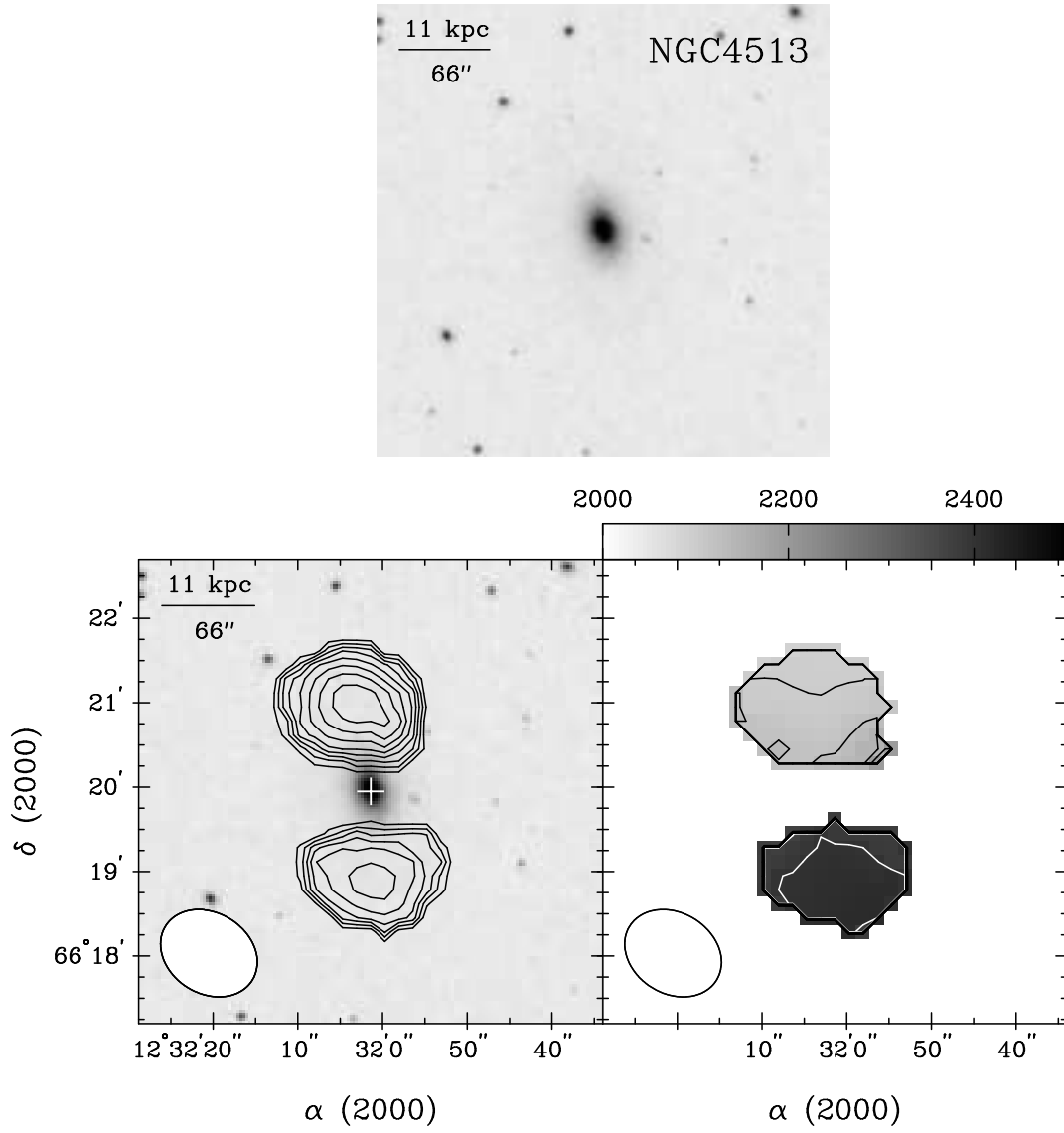


FIG. 18.— Upper panel: Optical image of NGC 4513 (Control sample) from the DSS2. Lower panels: (*Left*) Contours of zeroth moment overlaid on the DSS2 image, and (*Right*) first moment map. In the zeroth moment map, contours are plotted at 3, 6, 9, 12, $15 \times 31.2 \text{ mJy beam}^{-1} \text{ km s}^{-1}$ ($1.2 \times 10^{19} \text{ cm}^{-2}$). The half-power width of the synthesized beam has a size of $73'' \times 57''$.

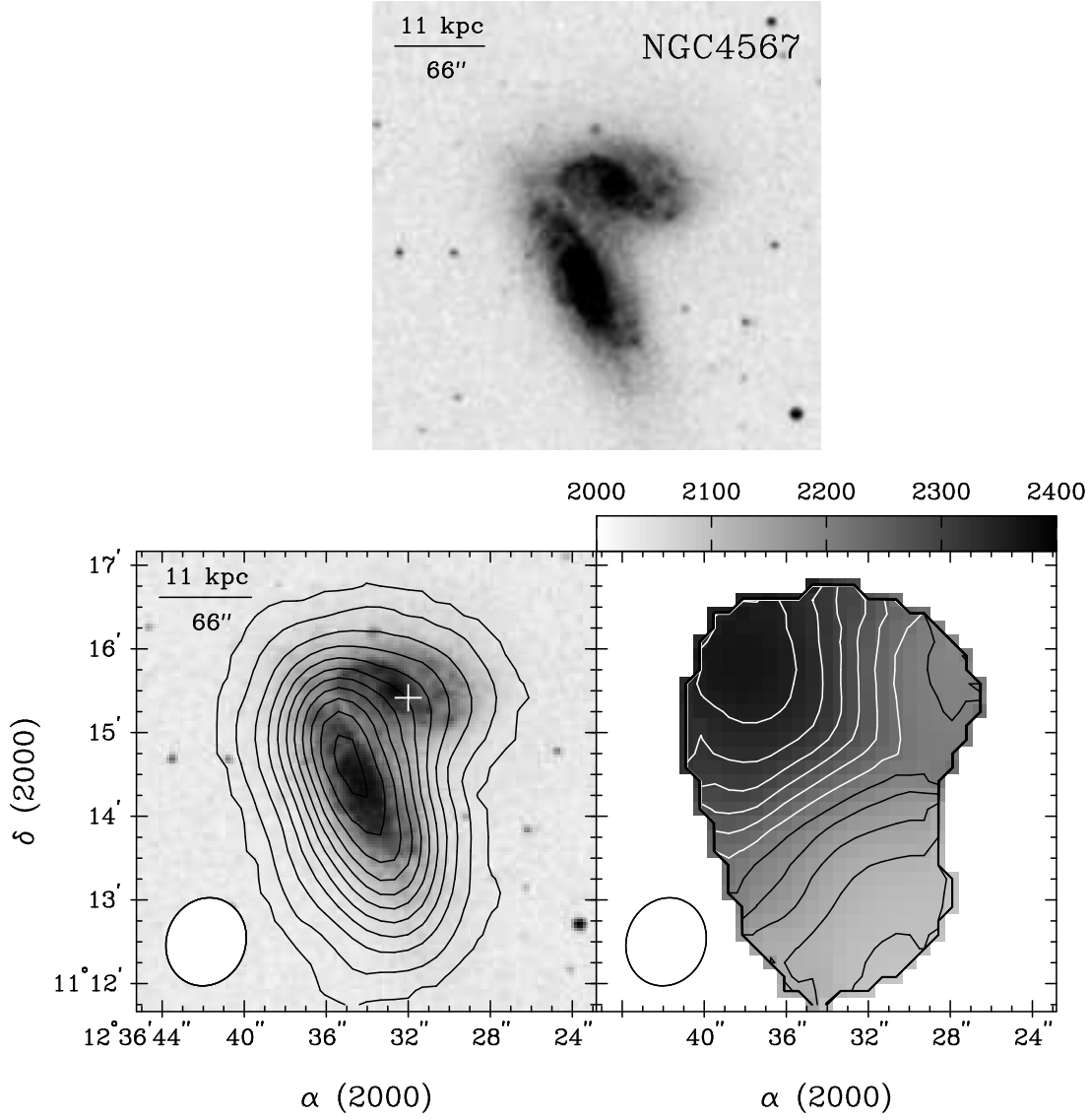


FIG. 19.— Upper panel: Optical image of NGC 4567 (Control sample) from the DSS2. Lower panels: (*Left*) Contours of zeroth moment overlaid on the DSS2 image, and (*Right*) first moment map. In the zeroth moment map, contours are plotted at 3, 20, 40, 60, $80 \times 24.8 \text{ mJy beam}^{-1} \text{ km s}^{-1}$ ($1.1 \times 10^{19} \text{ cm}^{-2}$). The half-power width of the synthesized beam has a size of $64'' \times 57''$.

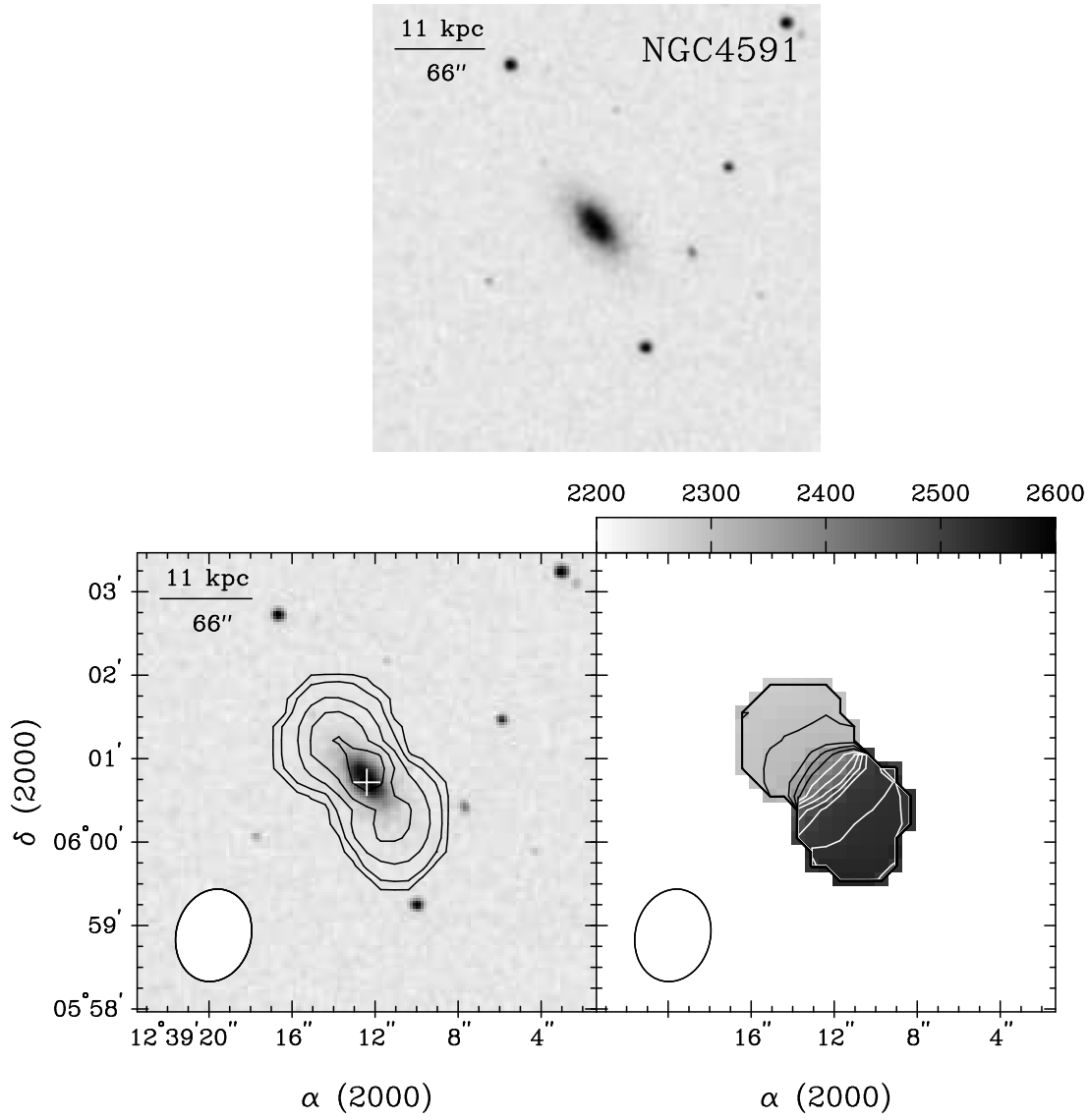


FIG. 20.— Upper panel: Optical image of NGC 4591 (Control sample) from the DSS2. Lower panels: (*Left*) Contours of zeroth moment overlaid on the DSS2 image, and (*Right*) first moment map. In the zeroth moment map, contours are plotted at 3, 10, 20, 30, $40 \times 24.0 \text{ mJy beam}^{-1} \text{ km s}^{-1}$ ($1.1 \times 10^{19} \text{ cm}^{-2}$). The half-power width of the synthesized beam has a size of $67'' \times 54''$.

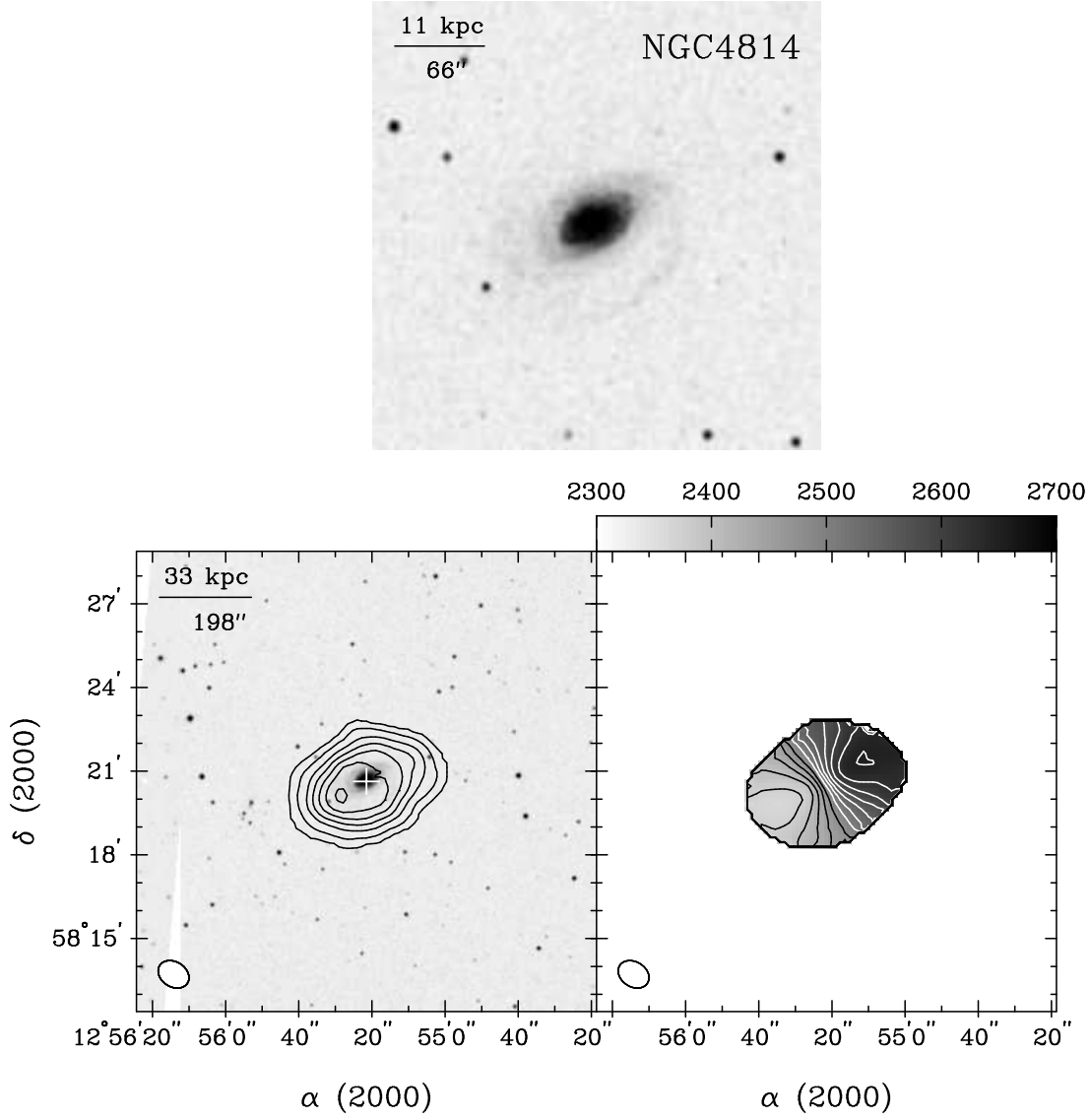


FIG. 21.— Upper panel: Optical image of NGC 4814 (Control sample) from the DSS2. Lower panels: (*Left*) Contours of zeroth moment overlaid on the DSS2 image, and (*Right*) first moment map. In the zeroth moment map, contours are plotted at 3, 10, 20, 30, 40 \times 46.1 mJy beam⁻¹ km s⁻¹ (2.0×10^{19} cm⁻²). The half-power width of the synthesized beam has a size of $71'' \times 54''$.

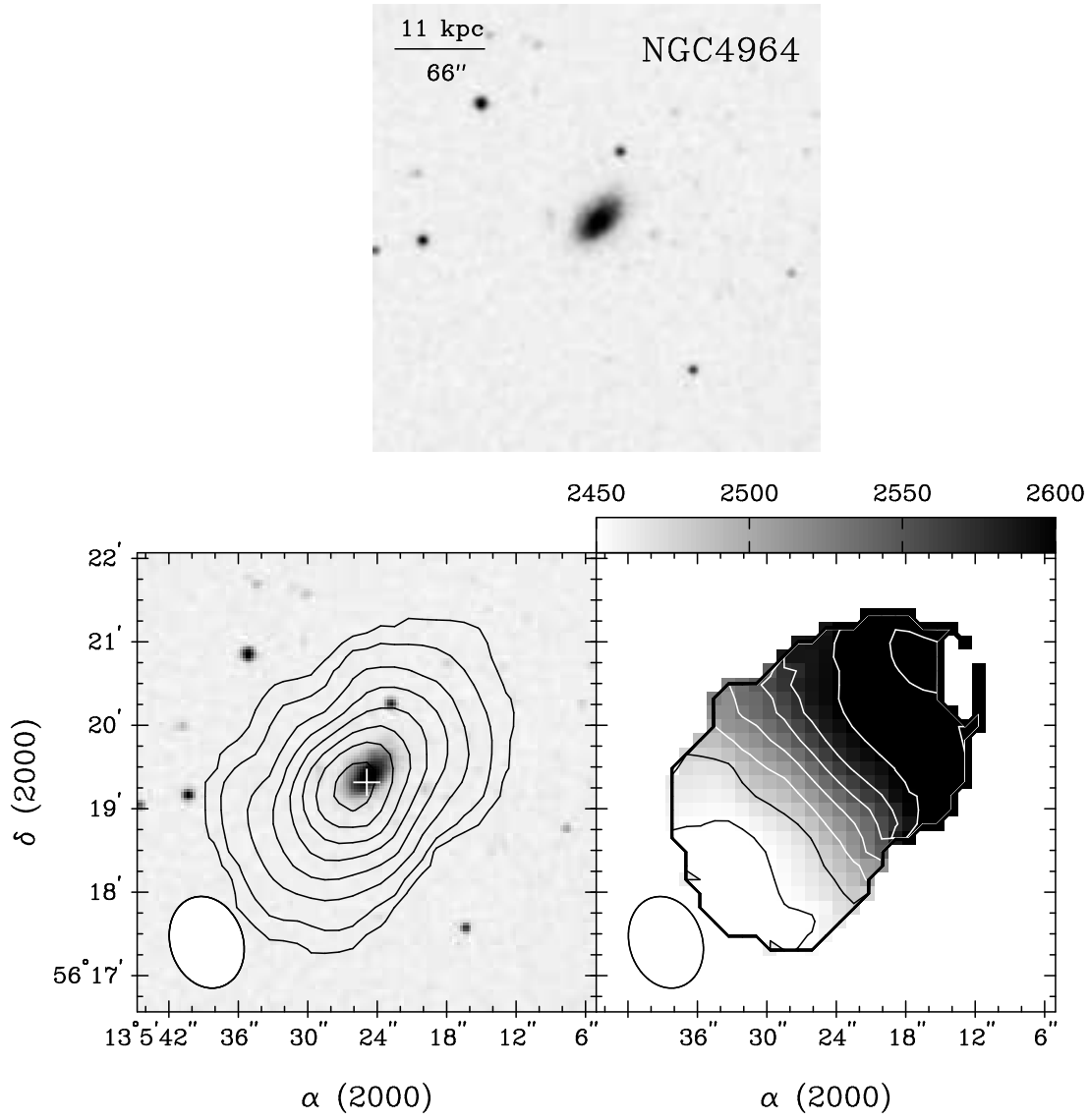


FIG. 22.— Upper panel: Optical image of NGC 4964 (Control sample) from the DSS2. Lower panels: (*Left*) Contours of zeroth moment overlaid on the DSS2 image, and (*Right*) first moment map. In the zeroth moment map, contours are plotted at 3, 10, 20, 30, $40 \times 29.4 \text{ mJy beam}^{-1} \text{ km s}^{-1}$ ($1.4 \times 10^{19} \text{ cm}^{-2}$). The half-power width of the synthesized beam has a size of $67'' \times 52''$.

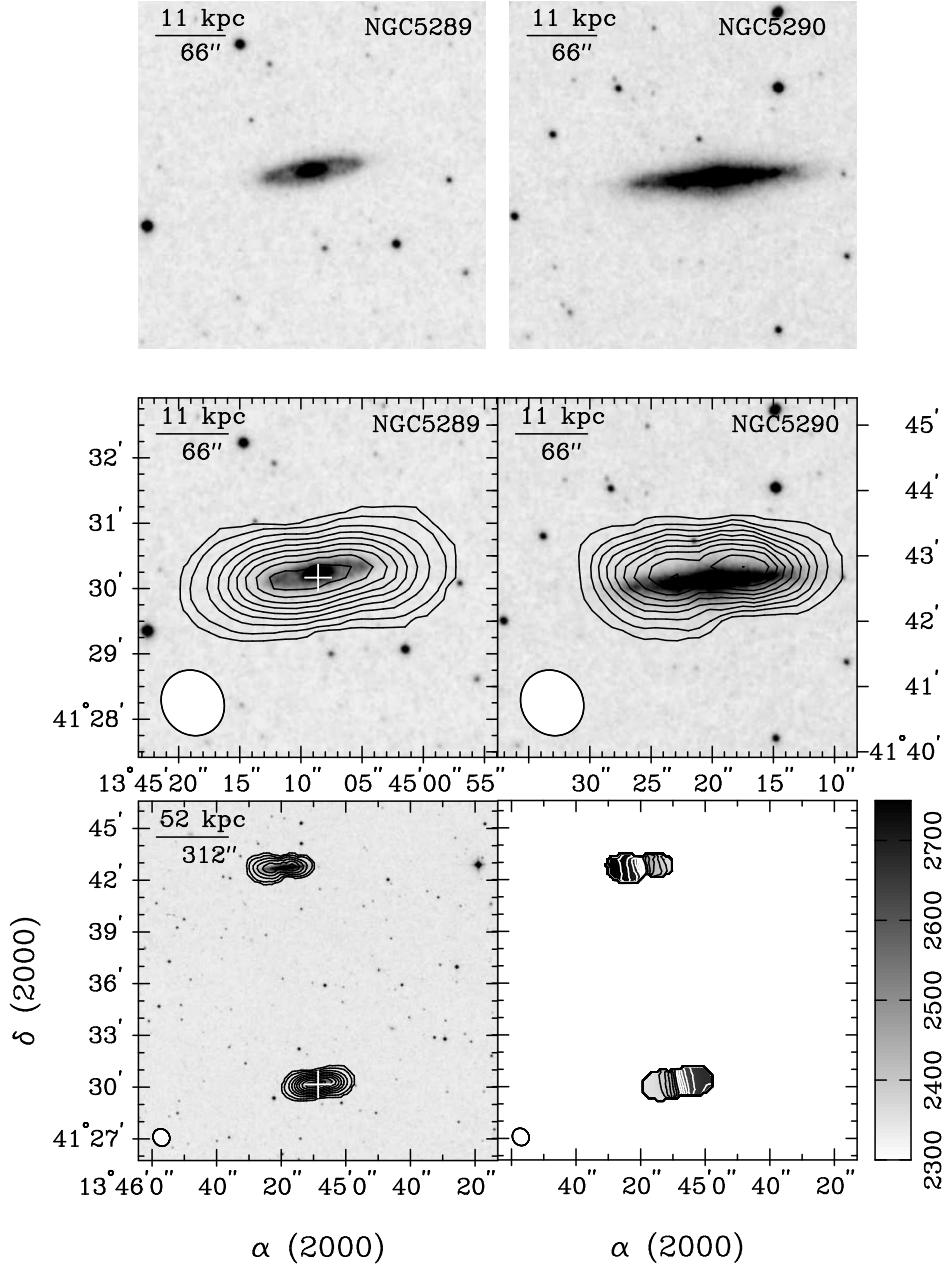


FIG. 23.— Upper panel: Optical image of NGC 5289 (Control sample) and NGC 5290 from the DSS2. Middle panels: Contours of zeroth moment overlaid on the DSS2 image. Lower panels: (*Left*) Contours of zeroth moment overlaid on the DSS2 image and (*Right*) first moment map with larger field. In the zeroth moment maps, contours are plotted at $3, 10, 20, 30, 40 \times 20.8 \text{ mJy beam}^{-1} \text{ km s}^{-1}$ ($9.6 \times 10^{18} \text{ cm}^{-2}$). The half-power width of the synthesized beam has a size of $62'' \times 56''$.

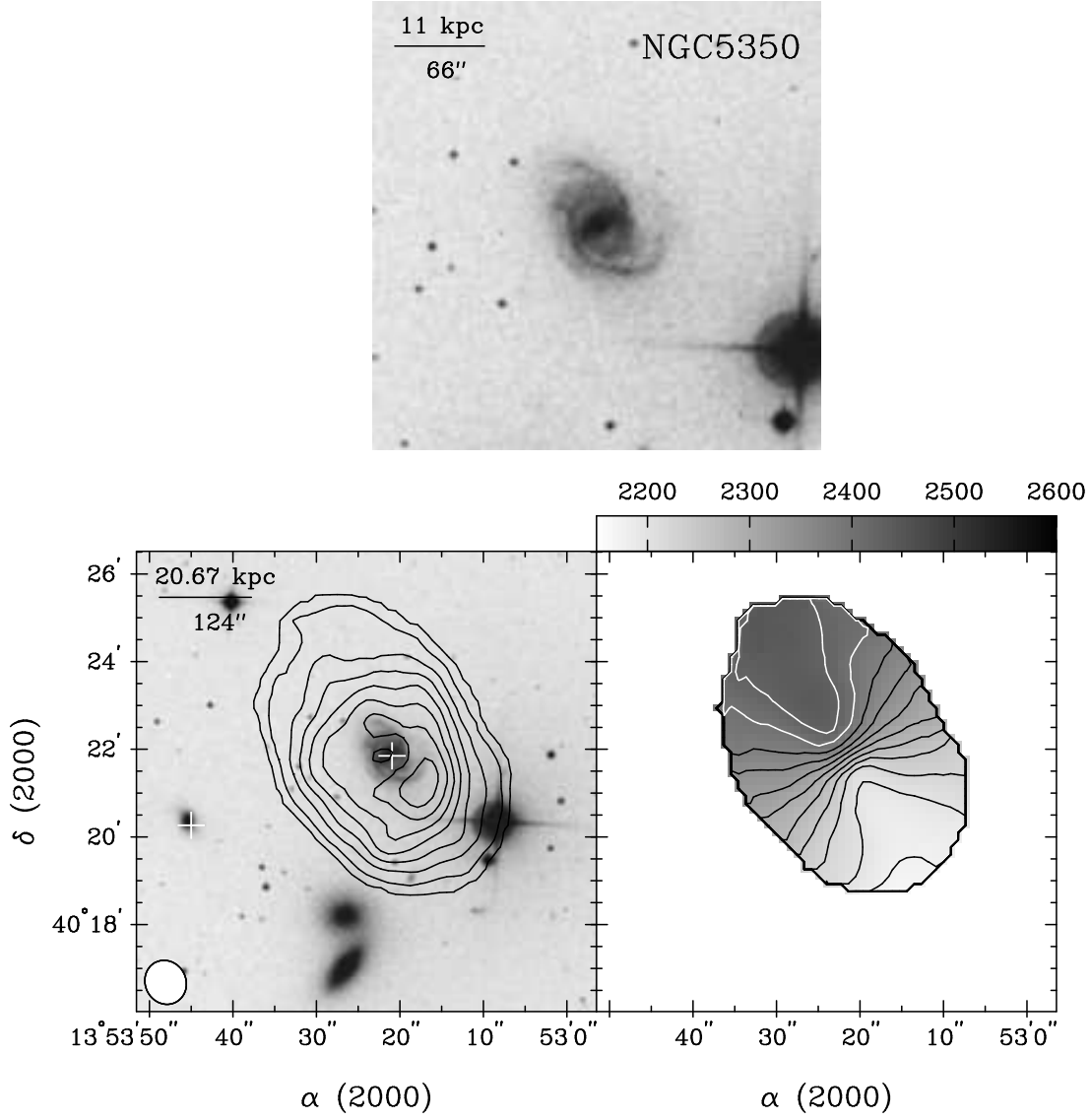


FIG. 24.— Upper panel: Optical image of NGC 5350 (Control sample) from the DSS2. Lower panels: (*Left*) Contours of zeroth moment overlaid on the DSS2 image, and (*Right*) first moment map. In the zeroth moment map, contours are plotted at 3, 10, 20, 30, $40 \times 31.8 \text{ mJy beam}^{-1} \text{ km s}^{-1}$ ($1.5 \times 10^{19} \text{ cm}^{-2}$). The half-power width of the synthesized beam has a size of $61'' \times 56''$.

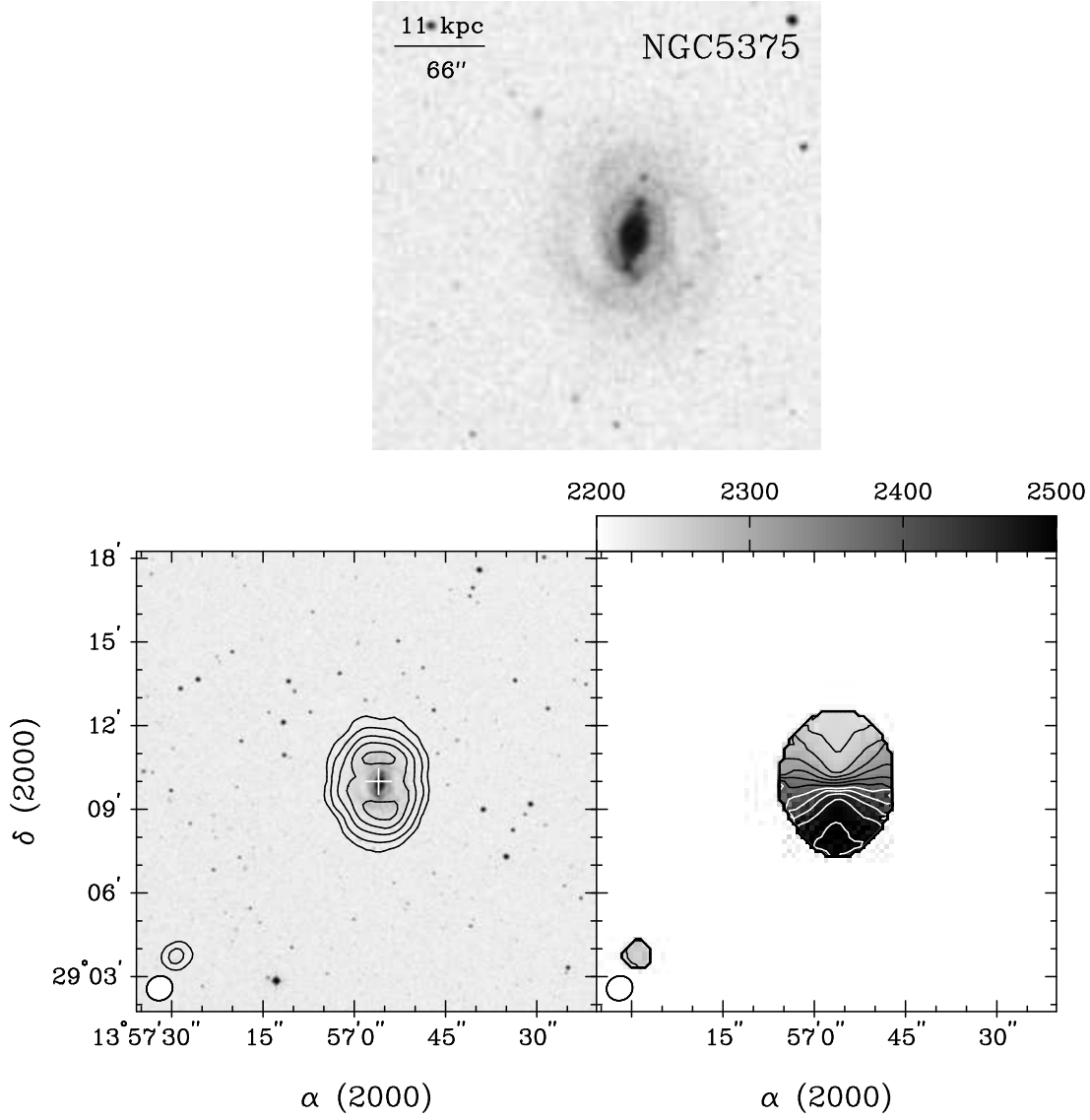


FIG. 25.— Upper panel: Optical image of NGC 5375 (Control sample) from the DSS2. Lower panels: (*Left*) Contours of zeroth moment overlaid on the DSS2 image, and (*Right*) first moment map. In the zeroth moment map, contours are plotted at 3, 10, 20, 30, 40 \times 32.3 mJy beam⁻¹ km s⁻¹ (1.8×10^{19} cm⁻²). The half-power width of the synthesized beam has a size of $57'' \times 52''$.

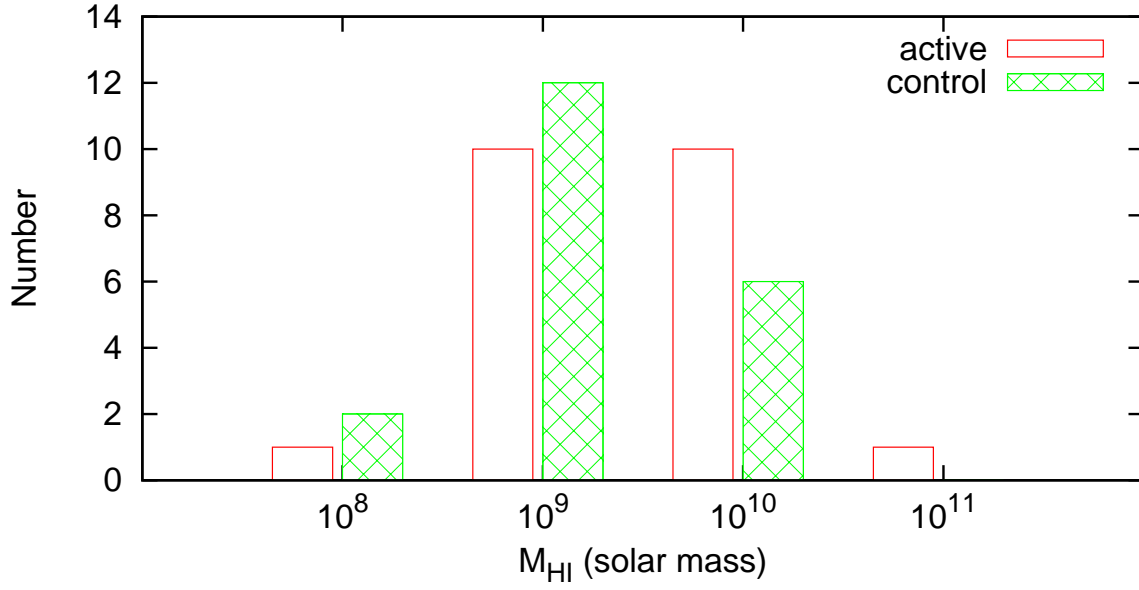


FIG. 26.— Distribution in HI gas masses of ensemble active galaxy sample of Kuo et al. (2008) (solid histogram) and our ensemble control sample (hatched histogram). The combined HI gas masses of NGC 4567/NGC 4568 in the control sample is plotted.

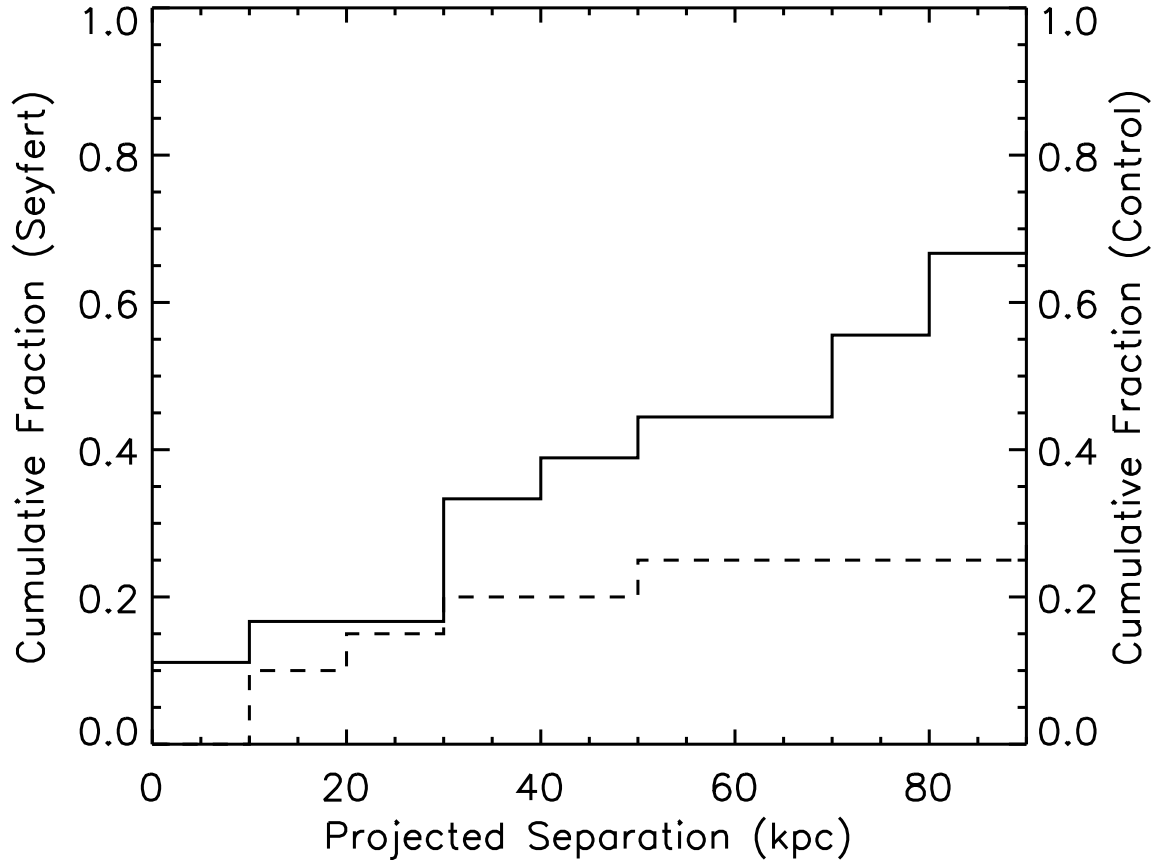


FIG. 27.— Cumulative fraction of Seyfert galaxies (solid line) and control sample (dashed line) with interacting neighboring galaxies plotted as a function of their projected separations.